1-1-2017

Synaptotagmin C2b Ca2+-Binding Loops Impose Distinct Exocytosis Phenotypes

Michael W. Schmidtke
Wayne State University,

SYNAPTOTAGMIN C2B CA^{2+}-BINDING LOOPS IMPOSE DISTINCT EXOCYTOSIS PHENOTYPES

by

MICHAEL W. SCHMIDTKE

THESIS

Submitted to the Graduate School

of Wayne State University,

Detroit, Michigan

in partial fulfillment of the requirements

for the degree of

MASTER OF SCIENCE

2017

MAJOR: BIOLOGICAL SCIENCES

(Cellular, Developmental, & Neurobiology)

Approved By:

_____

Advisor Date

DEDICATION

To my loving wife, Christina and our little bun in the oven.

ACKNOWLEDGMENTS

I would first like to thank my committee members. In particular, I am grateful to my research advisor, Dr. Arun Anantharam, for his intellectual support, research funding, and willingness to take me on as a graduate student in his lab. I am also indebted to my thesis advisor, Dr. Karen Beningo, for her guidance and motivation during the preparation of my thesis and oral presentation. Additional thanks go to Dr. David Njus and Dr. Joy Alcedo for their thoughtful suggestions pertaining to my writing and data analysis. Furthermore, I am grateful to Dr. Edward Golenberg and Ms. Rose Mary Priest of the Wayne State University biology department for their commitment to student success and administrative assistance.

Special thanks go out to my former lab colleagues, Dr. Tejeshwar Rao and Mr. Peter Dahl, for the many constructive conversations and late nights spent working together. I would not be where I am today without your encouragement and camaraderie through the years.

Finally, I am grateful to my family for their persistent support and unwavering confidence in my abilities. Thank you to my parents, Mark and Julie Schmidtke, for instilling in me the integrity to handle any situation, and to my wife, Christina, for having the patience to deal with the trials and tribulations of graduate student life.

TABLE OF CONTENTS

LIST OF FIGURES

LIST OF TABLES

CHAPTER 1 – BACKGROUND INFORMATION

Overview of Exocytosis

Exocytosis and the molecular machines that are involved in carrying out this essential cellular process, are complex and poorly understood. In its most general sense, exocytosis is the process by which a cell releases a portion of its contents to the external surface of its membrane. This is achieved by the trafficking and subsequent merging of cytoplasmic, membrane-bound vesicles with the plasma membrane. Exocytosis is critical for the survival of nearly all cell types, where its precise role is defined by the vesicular contents. For example, synaptic vesicles in neurons contain small, water-soluble neurotransmitters that are used to transmit signals from one neuron to another throughout the body. Similarly, a special class of neuroendocrine cells found in the pancreas contain vesicles pre-loaded with the peptide hormone insulin, which is released into the blood stream to help sequester glucose. However, exocytosis is not used exclusively for the release of cargo, it is also used for maintaining components of the cell's plasma membrane. Various lipid molecules and membrane associated proteins that form the vesicle membrane will become continuous with the plasma membrane during exocytosis. For example, shuttling of cell surface receptors at a synapse is one of the primary ways that neurons can tune their response to incoming signals (long-term potentiation). The process of exocytosis should not be confused with the conceptually similar, yet functionally opposite process of endocytosis, which involves the uptake of extracellular materials into the cytoplasm of a cell.

Types of Exocytosis

Exocytosis can be broadly classified as either "constitutive exocytosis" or "regulated exocytosis". Constitutive exocytosis, is a process that occurs relatively continuously within cells

and does not require any externally induced "trigger" (Burgoyne & Morgan, 1993). This form of exocytosis maintains the appropriate lipid and protein content of a cell's plasma membrane, and releases extracellular matrix proteins (Alberts *et al*., 2008). Due to the importance of maintaining cell membrane composition, constitutive exocytosis is found in essentially all cell types throughout an organism. In contrast, regulated exocytosis is defined by the requirement for a stimulating signal to "trigger" the fusion of vesicle and plasma membranes (Burgoyne & Morgan, 1993). This triggering signal induces a sharp rise in the concentration of intracellular calcium (Ca^{2+}) and directs the molecular mechanisms leading to fusion of vesicle and plasma membranes. For this reason, regulated exocytosis is sometimes referred to as Ca^{2+}-dependent exocytosis. In intact tissue, the coordination of a triggering signal with a rise in intracellular Ca^{2+} requires specialized receptors and ion channels. Regulated exocytosis is typically employed for the release of biologically active signaling molecules from highly specialized cell types (e.g. neurons and neuroendocrine cells), because the triggering requirement allows for tight temporal regulation of a given signal.

During regulated exocytosis, once intracellular Ca^{2+} levels have spiked, the temporal dynamics of vesicle fusion with the plasma membrane can vary. Based on their timing, events are described as either "synchronous" or "asynchronous". Synchronous release refers to the portion of Ca^{2+}-induced exocytotic events that occur within tens of milliseconds of a transient spike in Ca^{2+} (i.e. these events are "synchronized" with the Ca^{2+} spike). On the other hand, asynchronous release events occur after a measurable delay and may continue to take place for up to a minute or more (Chow *et al.* 1992; Hagler and Goda, 2001; Yoshihara *et al*., 2010; Rao *et al.* 2014). In general, most exocytotic events (as much as 90% in neurons) are observed to be synchronous

(Kaeser and Regehr, 2014). However, many studies have suggested that in neuroendocrine cells, such as adrenal chromaffin cells, the temporal coupling is not as tight, resulting in more balance between synchronous and asynchronous fusion events (Chow *et al.* 1992; Voets *et al.*, 1999, Schonn *et al.*, 2008; Lefkowitz *et al.* 2014). The basis for this difference in time course is not well understood, but some have speculated that it is linked to vesicle populations sensing incoming Ca^{2+} differently. For example, this could be explained by vesicles differing in their proximity to Ca^{2+} entry points (Ca_V channels) and/or utilizing Ca^{2+} sensing proteins with different binding affinities (Li *et al.*, 1995; Chow *et al.*, 1996; Kaeser & Regehr, 2015).

Finally, after vesicles have initially fused with the plasma membrane, there is yet another distinction that can be made between the modes of exocytosis. The classic, or "Full collapse", fusion mode occurs when the vesicle membrane rapidly flattens into the plasma membrane, with the inner leaflet of the vesicle membrane becoming continuous with the outer leaflet of the plasma membrane and consequently releasing all vesicle contents to the extracellular space. In contrast, "kiss-and-run" (also called "cavicapture") exocytosis occurs when a fusing vesicle remains largely intact, with only a narrow fusion pore forming between the vesicle lumen and extracellular space. Following the persistence of this fusion pore, these vesicles may eventually undergo full collapse into the plasma membrane as described above, or alternatively their pore may reseal allowing the vesicle and remaining cargo to be recycled back into the cytoplasm (the defining property of "kiss-and-run"; Figure 1.1). It has been suggested that "kiss-and-run" exocytosis may be used by secretory cells as a means for conserving energy and limiting content release during basal conditions (i.e. homeostasis), while "full-collapse" may occur when there is an immediate need for abundant secretion (e.g. during a stress response). However, the

molecular mechanisms underlying these contrasting modes of exocytosis are not fully understood and will be a focus of this thesis.

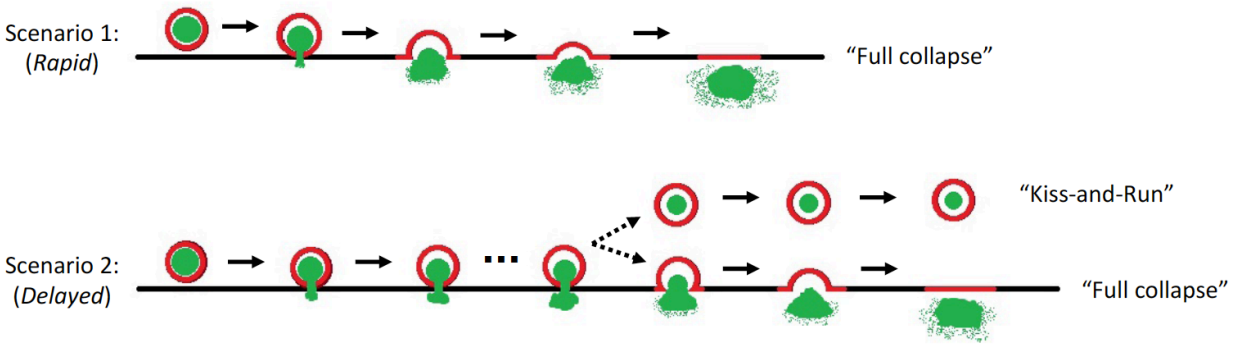

Figure 1.1: Modes of Exocytosis.
Following fusion of vesicle (red) and plasma membranes (black), exocytosis can proceed via two contrasting modes. The "classic" view of exocytosis (scenario 1) involves the vesicle membrane rapidly and completely collapsing into the plasma membrane, releasing all cargo from the vesicle. However, it is now known that some exocytotic events are characterized by the persistence of a narrow fusion pore (scenario 2) before the vesicle either fully collapses into the plasma membrane, or is endocytosed back into the cell retaining a portion of its cargo (kiss-and-run).

Steps of Regulated Exocytosis and Major Molecular Players

Regulated exocytosis in adrenal chromaffin cells occurs in four stages, and while many of the molecular players that orchestrate this process are known, a number remain to be discovered. These stages and select known players are described below.

Step 1: Docking

The first stage of exocytosis involves localizing secretory vesicles to the cytoplasmic region immediately adjacent to the plasma membrane (i.e. the subplasmalemmal space). Most studies classify vesicles as docked based on a morphological definition. On this basis, vesicles that are located within approximately 100 nm or less from the plasma membrane and exhibit minimal

lateral motion are considered "docked" (Steyer *et al.,* 1997; Verhage & Sorensen, 2008). In adrenal chromaffin cells, the typical density distribution of vesicles is appreciably higher in this subplasmalemmal space as compared to the rest of the cytoplasm, with one study estimating as much as a 20-fold increase in vesicle density in this region (Steyer *et al*., 1997).

One of the best understood molecules involved in vesicle docking is the protein Munc18-1. Munc18-1 is a cytosolic protein found in chromaffin cells and neurons that binds with high affinity to the SNARE protein Syntaxin-1 (discussed below) (Hata *et al.*, 1993). Chromaffin cells lacking Munc18-1 have a 10-fold reduction in the number of morphologically docked vesicles and reduced levels of Syntaxin-1 (Voets *et al.* 2001b). Syntaxin-1 is a transmembrane protein located on the inner surface of the plasma membrane and is one of the three essential Soluble *N*-ethylmaleimide-sensitive Factor Attachment Protein Receptor (SNARE) proteins involved in exocytosis. Corroborating its role in vesicle docking is the finding that Syntaxin-1 cleavage results in an approximately 7-fold reduction of docked vesicles (de Wit *et al*., 2006). Current models suggest that Munc18-1 binding to Syntaxin-1 acts to clamp the fusion-promoting SNARE complex in such a way that vesicles remain "tethered" near their eventual fusion sites (Gulyas-Kovacs *et al.*, 2007; Verhage & Sorensen, 2008; Sudhof & Rothman, 2009).

Step 2: Priming

In comparison to the visually perceivable process of docking, the priming step of exocytosis is more difficult to discern. While the exact proportion varies between studies, it is well established that only a subset of the total vesicles docked at the plasma membrane will undergo exocytosis. Priming converts vesicles from simply being docked at the membrane to becoming release competent (i.e. capable of undergoing fusion with the plasma membrane upon

experiencing a triggering spike in intracellular Ca^{2+}). This means a release-competent vesicle is not readily discernable until it has undergone exocytosis.

One of the earliest observations regarding priming of vesicles was the need for adenosine triphosphate (ATP) to convert morphologically docked vesicles into release competent vesicles (Holz *et al*., 1989). One of the proposed roles for ATP in the priming process involves resetting of the post-fusion SNARE complex via the ATPase, NSF. The core components of the fusion machinery are formed by three "SNARE" (or SNAP Receptor) proteins. Two of these proteins, Syntaxin-1 and Synaptosome-Associated Protein of 25 kDa (SNAP-25), are located on the plasma membrane (t-SNAREs), whereas the third protein, Synaptobrevin-2 (also called VAMP-2 for Vesicle-Associated Membrane Protein-2) is found inserted into the vesicle membrane (v-SNARE; Figure 1.2 A). The zippering of α-helical domains within these proteins provides the specificity and driving force for completing the process of exocytosis (Rothman 1994). Following a full-collapse fusion event, the three SNARE proteins are fully zippered together on the inside of the plasma membrane in what is termed the ternary *cis*-SNARE complex. Because this is an energetically favorable state, the SNARE components will remain twisted together, and thus unusable for future exocytosis, unless disassembled by an outside source. Disassembly of the *cis*-SNARE complex is achieved by the combined actions of cytoplasmic α-SNAP and *N*-ethylmaleimide-Sensitive Factor (NSF). NSF is an ATPase that utilizes ATP hydrolysis to unzip the α-helices of the SNARE proteins, thus returning them to their pre-fusion *trans* state (Sollner *et al.*, 1993; Hay & Scheller, 1997). The timing of this rearrangement process has been debated and may differ between cell types, but evidence from both chromaffin cells and PC12 cells (an immortalized chromaffin cell line) suggests that ATP-dependent NSF-mediated SNARE

disassembly occurs as part of the priming step leading up to exocytosis (Banerjeet *et al.*, 1996; Xu *et al.*, 1999).

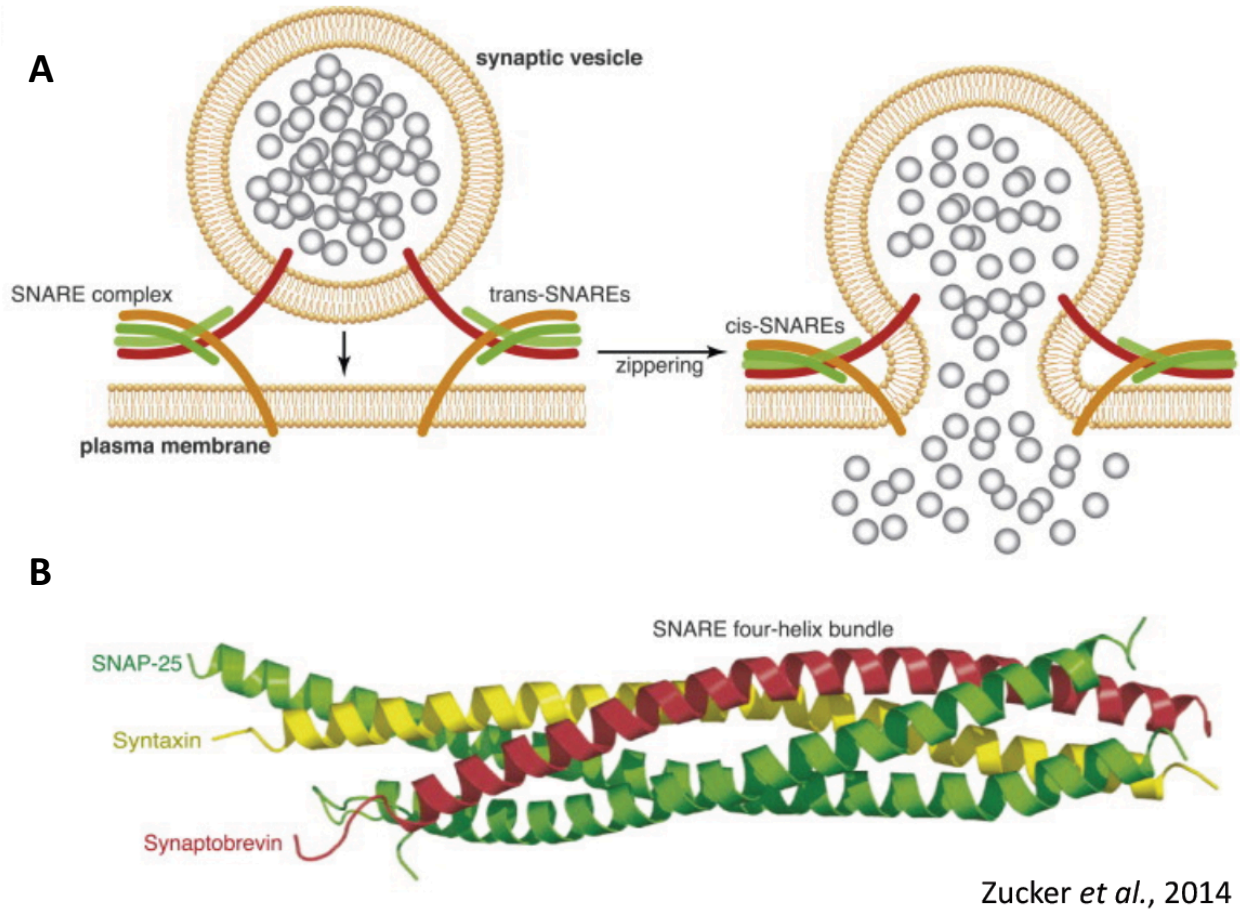

Figure 1.2: SNARE Complex Structure.
(A) Proposed arrangement of the SNARE complex between vesicle and plasma membranes. Synaptobrevin (dark red) is the sole vesicular SNARE (v-SNARE), with its N-terminus inserted into the vesicle membrane. Syntaxin (yellow) and SNAP-25 (green) are the target SNARES (t-SNARES), providing specificity for sites of exocytosis on the plasma membrane. Syntaxin contains an N-terminal transmembrane domain, whereas SNAP-25 is anchored to the inner leaflet of the plasma membrane via palmitoylation. **(B)** A single unit of the SNARE complex contains one copy each of Synaptobrevin and Syntaxin, along with two copies of SNAP-25. The primary driving force for exocytosis results from zippering of the four-helix bundle formed by a single α-helical contribution from each of the four SNARE molecules.

A second proposed role for ATP during vesicle priming is through the biosynthesis of Phosphatidylinositol 4,5-bisphosphate (PIP_2) from precursor molecules. PIP_2 is a negatively charged lipid molecule that is found on the inner leaflet of the plasma membrane at sites of exocytosis, and serves as a context-specific signal for binding of effector proteins (Holz *et al.*, 2000; Alberts *et al.*, 2008). Synthesis of PIP_2 involves the sequential conversion of Phosphatidylinositol (PI) to Phosphatidylinositol 4-phosphate (PIP) and then to PIP_2 by the ATP-dependent activity of Phosphatidylinositol 4-kinase (PI4KI) and Phosphatidylinositol 4-phasphate-5-kinase (PIP5KI), respectively. Proper trafficking of PIP_2 to the plasma membrane also involves the actions of Phosphatidylinositol Transfer Protein (PITP), a molecule shown to be required for ATP-dependent vesicle priming (Hay & Martin, 1993). An early study by Wiedemann *et al.* showed that inhibition of PIP_2, either directly or by blocking synthesis, resulted in fewer release competent vesicles in chromaffin cells (1996; Martin, 2012). More recent studies have confirmed the requirement for PIP_2 in vesicle priming and identified candidate effector molecules, including Ca^{2+}-Dependent Activator Protein for Secretion 1 (CAPS-1) and Munc13-1/2. These molecules bind to both PIP_2 and SNARE proteins, possibly serving to stabilize the SNARE complex prior to membrane fusion (Xu *et al.*, 1999; Martin, 2012; Kabachinski *et al.*, 2014). Furthermore, biochemical inhibition of either CAPS-1 or Munc13 will reduce the pool of release competent vesicles (Klenchin & Martin, 2000).

Step 3: Triggering

Once vesicles have become release competent, they sit poised at the plasma membrane until an appropriate triggering signal arrives. This triggering signal is ultimately manifest as a sharp rise in intracellular Ca^{2+} levels. In adrenal chromaffin cells, this Ca^{2+} spike results from

upstream signaling by acetylcholine (ACh) and Pituitary Adenylate Cyclase-Activating Peptide (PACAP), culminating in the opening of voltage-gated Ca^{2+} (Ca_V) channels in the plasma membrane (Smith & Eiden, 2012). Ca^{2+} entry triggers exocytosis by acting on members of the Ca^{2+}-binding Synaptotagmin (Syt) protein family (Perin *et al.*, 1990; Brose *et al.*, 1992; Tucker & Chapman, 2002). Although there are many isoforms of Syt, chromaffin cells only express Syt-1 and Syt-7 (Schonn *et al.*, 2008). These Syt isoforms are transmembrane proteins found on secretory vesicles and contain two cytoplasmic Ca^{2+}-binding domains (see below). Loss of Syt-1 and/or Syt-7 will reduce synchronous and asynchronous Ca^{2+}-triggered vesicle fusion respectively, implicating these proteins as the Ca^{2+} sensors for regulated exocytosis (Geppert *et al.*, 1994; Voets *et al.*, 2001a; Schonn *et al.*, 2008; Bacaj *et al.*, 2013).

Once bound by Ca^{2+}, Syt may act to promote the downstream fusion process through multiple mechanisms. First, there is evidence that Ca^{2+}-bound Syt can bind with, and partially insert itself into, membranes containing PIP_2 (Martens *et al.*, 2007; Lynch *et al.*, 2008). This interaction may induce positive plasma membrane curvature that promotes merging with the closely apposed vesicle membrane (Hui *et al.*, 2009). Secondly, Ca^{2+}-bound Syt has been shown to bind the t-SNARE proteins Syntaxin-1 and SNAP-25 as well as the cytoplasmic protein Complexin. Multiple studies have shown that mutations disrupting the Ca^{2+}-mediated binding of Syt-1 to t-SNAREs inhibits SNARE-induced vesicle fusion both *in vitro* (Bhalla *et al.*, 2005; 2006) and *in vivo* (Martens *et al.*, 2007; Lynch *et al.*, 2008). Thus, it has been proposed that Syt-SNARE binding may facilitate assembly or stabilization of the SNARE complex as it drives membrane fusion. Evidence also suggests that the soluble protein Complexin plays an important role during Syt-mediated triggering of exocytosis. It is believed that Complexin acts as a “clamp”,

simultaneously binding the t-SNARE Syntaxin-1 and v-SNARE Synaptobrevin-2 to prevent premature zippering of α-helices and concomitant vesicle fusion. Consistent with this model, Ca^{2+}-bound Syt may act by binding Complexin and removing it from the SNARE complex, thereby releasing the inhibitory "clamp" and allowing fusion to proceed (Tokumaru *et al.*, 2008). These mechanisms are not mutually exclusive, and therefore might act together to trigger exocytosis. Recently, a third mechanism for triggering of fusion was proposed based on the tendency for Syt to form homo-oligomers *in vitro*. This explanation suggests that prior to Ca^{2+} entry, a ring-like chain of Syt molecules could act as a spacer between the vesicle and plasma membranes, preventing further zippering of the SNARE complex until the ring disassembles in the presence of Ca^{2+} (Wang *et al.*, 2014). However, this mechanism has yet to be proven *in vivo*, and therefore requires further investigation to assess its validity.

Step 4: Fusion

The final and most conspicuous step of exocytosis is the actual fusion of vesicle and plasma membranes. As discussed above, myriad evidence supports the theory that membrane fusion is specified and driven by the energetically favorable zippering of α-helical domains within the transmembrane v- and t-SNARE proteins – a concept referred to as the "SNARE hypothesis" (Rothman, 1994). Crystal structure analysis of the SNARE complex revealed that the cytoplasmic portion is composed of four α-helices; Synaptobrevin-2 and Syntaxin-1 each contribute a single helix, whereas two copies of SNAP-25 contribute one helix each (Sutton *et al.*, 1998; Figure 1.2 B). While this four-helix bundle serves as a basic unit of the SNARE complex, it is still unclear how many copies of this structure are associated with a typical exocytotic event. Prior to fusion, v-SNAREs and t-SNAREs are found on separate membranes, and therefore referred to as a *trans*-

SNARE complex. Following α-helix zippering and full-collapse of the vesicle membrane into the plasma membrane, all SNAREs are located together on the same membrane, referred to as the *cis*-SNARE complex (also called the ternary complex since it is composed of three tightly coiled protein species). Disassembly of the *cis*-complex is required before SNAREs can be recycled to their respective membranes for use in another round of exocytosis, and this is achieved by the combined actions of the cytoplasmic proteins NSF and α-SNAP (Sollner *et al.*, 1993; Hay & Scheller, 1997).

It was originally thought that once the vesicle and plasma membranes initially fused with one another to form a fusion pore, exocytosis would always proceed rapidly with full-collapse of the vesicle into the plasma membrane (Heuser *et al.*, 1979; Chow *et al.*, 1992). However, more recent work has established a contrasting mode known as "kiss-and-run" fusion, where the fusion pore may persist for tens-of-seconds before resealing as a form of endocytosis (Fesce *et al.*, 1994; Taraska *et al.*, 2003; Harata *et al.*, 2006; Rao *et al.*, 2014). Many proteins have been suggested to influence the rate of fusion pore expansion (or the lack thereof), including the Ca^{2+} sensor Synaptotagmin. However, the basis for how Syt influences pore expansion, and thus fusion mode, is currently unknown.

The Adrenal Chromaffin Cell

Chromaffin cells, named by Alfred Kohn for their chromium salt affinity (used for staining), are the primary cell type found in the adrenal medulla. These cells are best known for their physiological role in producing and secreting the catecholamines epinephrine (adrenaline) and norepinephrine in the context of the mammalian "fight-or-flight" response originally described by Walter B. Cannon. Chromaffin cells serve as the primary effector in the Hypothalamo-

Splanchnico-Adrenomedullary (HSA) axis, receiving input from the greater splanchnic nerves (part of the sympathetic nervous system) (Carmichael & Winkler, 1985). In response to acetylcholine (ACh) and Pituitary Adenylate Cyclase-Activating Peptide (PACAP) signaling from the splanchnic nerves, chromaffin cells release a variety of physiologically relevant substances via both synchronous and asynchronous exocytosis (Voets *et al.*, 1999; Smith & Eiden 2012). These substances include: epinephrine (Epi), norepinephrine (NE), neuropeptide Y (NPY), tissue plasminogen activator (tPA), enkephalin, and chromogranins A & B (CgA, CgB) (Lundberg *et al.*, 1979; Carmichael & Winkler, 1985; Coupland, 1989). The functional roles of these molecules range from increasing heart rate and blood pressure (Epi & NE), to breaking down blood clots (tPA), and even inducing analgesia (enkephalin). Substances to be released from chromaffin cells are loaded into large dense-core vesicles (LDCVs), named for their large size (~300 nm) relative to synaptic vesicles and visually darkened center resulting from peptide aggregations (e.g. CgA). LDCVs occupy most of the cytoplasm, and single chromaffin cells have been estimated to contain upwards of 30,000 individual vesicles (Carmichael & Winkler, 1985; Figure 1.3).

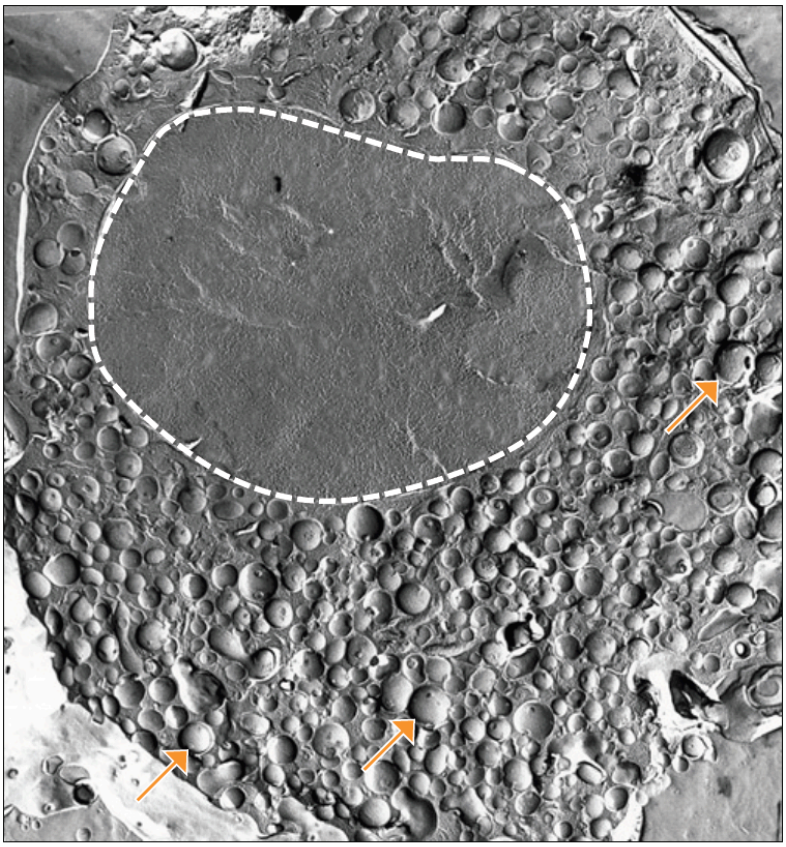

Carmichael & Winkler, 1985

Figure 1.3: Chromaffin Cell Large Dense-Core Vesicles (LDCVs).
Electron micrograph from freeze fracture of a chromaffin cell revealing the relative size and high density of large dense-core vesicles (LDCVs) in the cytosol. Nucleus (white dashed circle) surrounded by the cytosol packed full of LDCVs (orange arrows) with approximate diameters of ~300 nm. Image credit to Wolfgang Schmidt of the University of Innsbruck, Austria.

The size and abundance of LDCVs in chromaffin cells, along with the relative ease with which these cells can be isolated and maintained in primary culture, make the chromaffin cell an ideal model for studying the properties of exocytosis. Their large size and lack of morphological processes make chromaffin cells easier to viably dissociate from living tissue as compared to neurons (Kolski-Andreaco *et al.*, 2007). Once isolated in 2-dimensional culture, these cells take on a roughly spherical shape that makes them amenable to a variety of imaging and electrophysiological techniques, such as patch clamping (Fenwick *et al.*, 1982; Anantharam *et al.*,

2010). Furthermore, chromaffin cells can survive in culture for a week or more, allowing them to be isolated in large batches and subsequently used in multiple experiments.

A Closer Look at the Calcium Sensor Synaptotagmin

As discussed above, Synaptotagmin (Syt) is widely accepted to be the primary Ca^{2+}-sensing protein that triggers regulated exocytosis in neurons and neuroendocrine cells (Brose *et al.*, 1992; Sudhof & Rizo, 1996; Tucker & Chapman, 2002). Syt was first identified as p65 in a protein screen of synaptic vesicles from rat neurons (Perin *et al.*, 1990). The most salient feature of p65 was its ability to bind Ca^{2+} ions and acidic phospholipids. Binding sites for these molecules are located in two cytoplasmic domains that share a high degree of sequence homology with the Ca^{2+}-binding C2 domain of protein kinase C (PKC). To date, as many as 17 isoforms of Syt have been identified in the mammalian genome, with all family members sharing a common structure containing an N-terminal transmembrane domain, followed by the tandem C2 domains (referred to as C2A and C2B) connected by a short linker region (Sudhof & Rizo, 1996; Sudhof, 2002; Gustavsson & Han, 2009; Bacaj *et al,*. 2013; Figure 1.4, A-C).

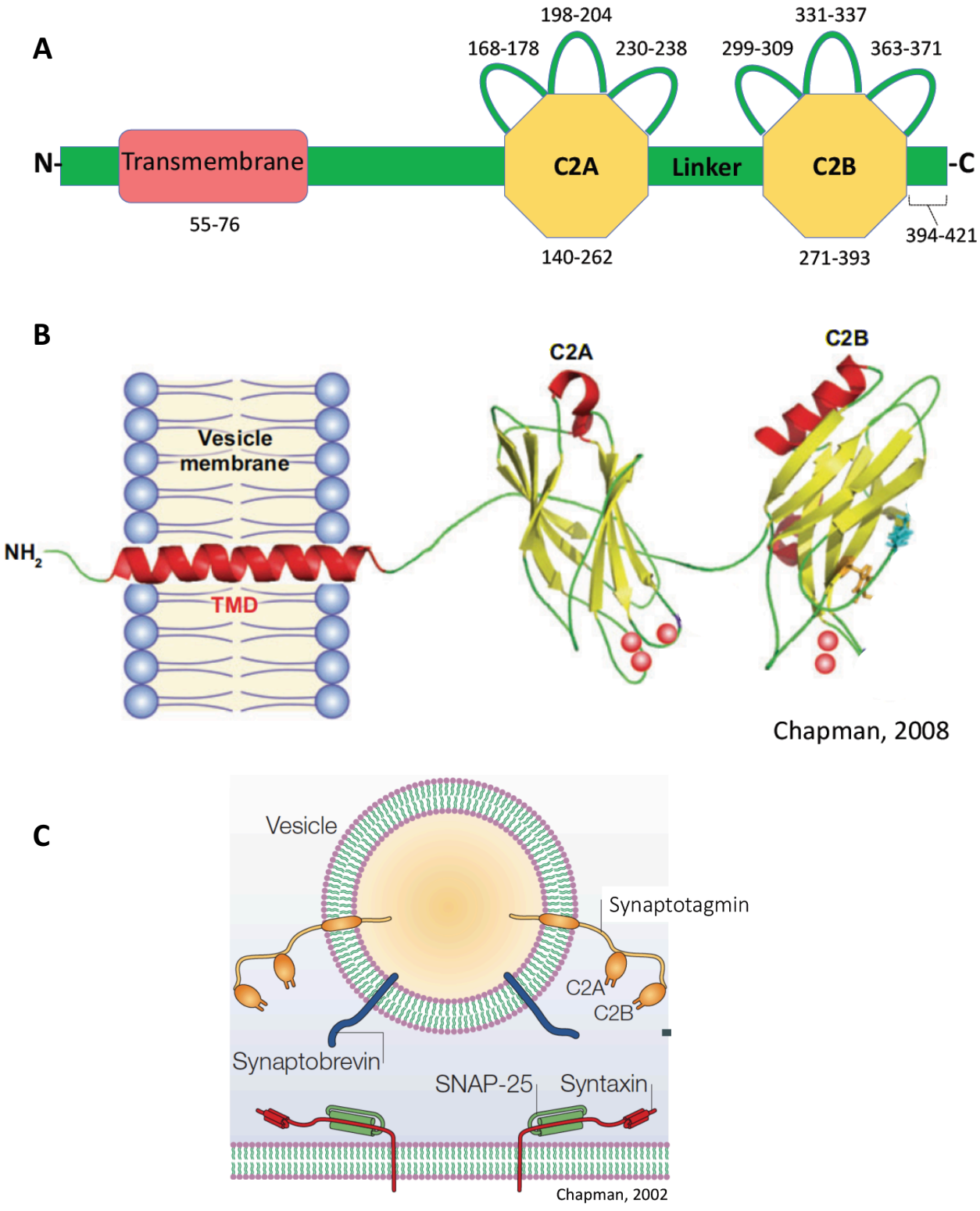

Figure 1.4: Synaptotagmin Structure.
(A) Simplified domain structure of Synaptotagmin, showing the relative position of the transmembrane domain (red) and Ca^{2+}-binding C2A and C2B domains (yellow), each containing

three Ca^{2+}-binding loops (green). A short linker connects the C2A and C2B domains (green). Amino acid ranges are listed for Syt-1 based on Chapman *et al.*, 1996 and Sudholf & Rizo, 1996. **(B)** Ribbon diagram of Syt-1. The transmembrane domain (TMD; red) is a single α-helix, whereas the C2 domains are each composed of a β-sandwich (yellow) with Ca^{2+}-binding loops extending out from the edge (green). Bound Ca^{2+} ions are depicted as red spheres. Image modified from Chapman, 2008. **(C)** Position of Syt in the vesicle membrane at an exocytotic site. The C2A and C2B domains hang into the cytosol, poised to interact with the plasma membrane and SNARE complex upon Ca^{2+} binding. Image from Chapman, 2002.

Each C2 domain of Syt is composed of two stacked β-sheets (i.e. a β-sandwich) with three flexible loops extending out from the top and bottom (Sutton *et al.*, 1995; Sudhof & Rizo, 1996). The Ca^{2+}-binding ability of Syt is generally attributed to the interaction of positively charged Ca^{2+} ions with five negatively charged aspartic acid (Asp, D) residues found in the top loops of each C2 domain (Fernandez-Chacon *et al.*, 2002). Binding of Syt to anionic phospholipids also appears to be dependent on these Asp residues and likely occurs due to the electrostatically favorable "bridge" that Ca^{2+} ions form between the negatively charged phospholipid head groups and C2 domain Asp residues (Zhang *et al.*, 1998). Furthermore, membrane binding is thought to be enhanced by other amino acid residues present in the C2 loops that possess either a positive charge (Lys, Arg) or hydrophobic side chain (Met, Phe, Val, Ile) (Frenandez-Chacon *et al.*, 2002). It is worth mentioning that not all Syt isoforms bind Ca^{2+} or phospholipids with their C2 domains, and this is likely due to the observed absence of the critical Asp residues (Gustavsson & Han, 2009).

Seminal Synaptotagmin Findings and Resulting Questions

Following the discovery and structural characterization of Syt, a number of important studies were conducted that paved the way for the current thesis research. Although many isoforms of Syt are found in the mammalian genome and expressed in various parts of the body,

the finding that only Syt-1 and Syt-7 are expressed in the physiologically important chromaffin cell (Schonn *et al.*, 2008) raised an important question – are these isoforms interchangeable in their physiological roles, or do they possess unique properties allowing them to be employed in divergent contexts? Sugita *et al.* (2002) were the first to compare the relative Ca^{2+} affinities of various Syt isoforms *in vitro*, concluding that Syt-7 showed ~10-fold higher affinity for Ca^{2+} than Syt-1. This finding was taken one step further by Bhalla *et al.* (2005) who compared the ability of the Syt-1 and Syt-7 cytoplasmic domains (which include both C2A and C2B) to promote SNARE-mediated vesicle fusion *in vitro*. Using their fusion assay, they observed that Syt-7 stimulated membrane fusion in the presence of roughly 400-fold less Ca^{2+} than Syt-1, indicating that at least *in vitro* these isoforms can couple exocytosis to drastically different concentrations of Ca^{2+}. Furthermore, concurrent research by the same lab provided evidence that Syt-1 dissociates from lipid surfaces more than 10x faster than Syt-7 *in vitro*, suggesting that Syt-1 and Syt-7 may act separately to mediate synchronous and asynchronous release respectively (Hui *et al.*, 2005). In the wake of these *in vitro* biochemical studies, Schonn *et al.* (2008) provided early evidence for this theory by investigating the effects of Syt-1 or Syt-7 knockout on vesicle release kinetics using cultured mouse chromaffin cells. They found that Syt-1 KO resulted in a substantial decrease in fast, synchronous exocytosis (in agreement with Voets *et al.*, 2001a), while Syt-7 KO led to an increase in the fast component (most likely due to the loss of slower, asynchronous exocytotic events).

These early studies provided the first hints at a potential mechanism for how chromaffin cells might utilize their two versions of Syt to tune the release kinetics of vesicular cargo. However, taken together these findings also raised a series of new questions regarding the

molecular regulation of exocytotic fusion modes in chromaffin cells. For example, do individual LDCVs contain copies of both Syt-1 and Syt-7, or are these isoforms sorted to different vesicle populations? If the latter is true, do the distinct biochemical Ca^{2+} and lipid-binding properties of each isoform translate into differences in how (i.e. fusion mode) and when each vesicle population is activated to undergo exocytosis? Furthermore, if there are differences in the preferred fusion mode of Syt-1 versus Syt-7, does this alter the release rate of biologically active cargo molecules from vesicles?

To begin to address these questions, Zhang *et al.* (2011) performed a study examining the localization of Syt isoforms and their associated fusion mode in pheochromocytoma (PC12) cells – a cell line derived from tumorigenic chromaffin cells isolated from the rat adrenal medulla (Greene & Tischler, 1976). Although derived from normal chromaffin cells, PC12 cells differ in that they express four isoforms of Syt, including Syt-1, -4, -7, and -9 (Fukuda *et al.*, 2001; Tucker *et al.*, 2003; Ahras *et al.*, 2006). The study by Zhang *et al*. found that these four Syt isoforms are largely co-sorted in PC12 cells, with more than 60% co-localization between all isoform pairs except Syt-1/Syt-7 which showed significantly less overlapping distribution (~45%). More strikingly, the study also found that Syt-1 and Syt-7 appear to differ in their fusion kinetics. Using total internal reflection fluorescence (TIRF) microscopy (described below), the authors observed three types of fusion events: those that displayed rapid (<2 sec) loss of fluorescently-tagged Syt from fusion sites following exocytosis, those where loss of Syt occurred but was slower (>2 sec), and those where Syt fluorescence remained elevated indefinitely. Syt-1 fusion events were characterized by faster loss of Syt protein from sites of exocytosis, whereas Syt-7 events primarily displayed either slow loss or persistence of protein. The authors attributed these kinetic

differences to vesicles undergoing contrasting modes of fusion based on which Syt isoform they possessed. One important caveat of this study is the fact that it was conducted in PC12 cells as opposed to primary chromaffin cells. As with any immortalized cell line, PC12 cells are no longer under the selection pressures imposed by residence in an intact organism, and therefore it is possible that decades of subculturing have resulted in additional genomic alterations beyond those that led to their tumorigenic properties. For example, this could explain why two additional Syt isoforms are expressed in these cells and/or why these isoforms show a high degree of isoform co-sorting.

Rao *et al.* addressed the above concern by studying the localization and exocytotic phenotype of Syt-1 and Syt-7 in primary chromaffin cells isolated from bovine adrenal glands. Using an antibody-based approach, they found that Syt isoforms were independently sorted in these cells to a far greater degree than in PC12 cells, with less than 10% of vesicles expressing both isoforms (Rao *et al.*, 2014). Furthermore, overexpression of fluorescent Syt-pHluorin fusion proteins did not elevate the degree of co-localization. After establishing the differential sorting of Syt isoforms, the group looked at the Ca^{2+} requirements for stimulating exocytosis from each vesicle population.

As mentioned earlier, Ca^{2+} entry into chromaffin cells occurs via voltage-gated Ca^{2+} channels in the plasma membrane. While the voltage threshold for opening these channels is achieved through acetylcholine and PACAP receptor activation *in vivo*, this threshold can be surmounted in cell culture studies by bathing cells with solutions containing elevated cations, such as K^+. Solutions containing higher K^+ concentrations result in a greater influx of Ca^{2+} into cells (Fulop & Smith, 2007). Using a range of solutions containing various concentrations of KCl,

Rao *et al*. showed that moderate stimulation with 25 mM KCl (resulting in a mild rise in Ca^{2+}) specifically favored exocytosis by Syt-7 containing vesicles, while stronger depolarization with 56 mM KCl led to a slight preference for Syt-1 fusion over Syt-7. This finding, confirmed by additional methods in a follow-up study (Rao *et al.*, 2017), supports the idea that Syt-1 and Syt-7 endow their resident vesicle populations with distinct Ca^{2+} sensitivities, in agreement with their distinct biochemistries (Sugita *et al.*, 2002; Bhalla *et al.*, 2005).

Rao *et al.* also compared the fusion phenotype of Syt-1 versus Syt-7 vesicles in three ways using polarized TIRF (pTIRF) microscopy. This technique allows for simultaneous, real-time imaging of plasma membrane topography and fluorescent protein behavior (Anantharam *et al.*, 2010; see methods section for a complete description of this technique). First, examining the persistence of Syt at fusion sites, it was found that Syt-1 rapidly diffused while Syt-7 remained clustered for a minute or more (consistent with the PC12 findings of Zhang *et al.*, 2011). Second, using a combination of membrane topology and rapid bath solution pH switching, they showed that fusion pores associated with Syt-7 events tended to remain constricted for a minute or more, whereas those associated with Syt-1 quickly expanded until the vesicle membrane flattened into the plasma membrane (i.e. full-collapse). Nearly a third of all Syt-7 events resulted in endocytosis (i.e. kiss-and-run) during the imaging period, while only 8% of fusing Syt-1 vesicles were observed to follow the same fate. Finally, tracking the release rate of the abundant LDCV cargo protein Chromogranin B (CgB) revealed that it is released significantly faster from Syt-1 as opposed to Syt-7 vesicles. Recently this effect of Syt isoforms on cargo release rates has been reaffirmed using the appreciably smaller cargo molecule Neuropeptide Y (NPY) (Rao *et al.*, 2017).

In summation, the study by Rao *et al.* (2014), along with those preceding it, have painted a potential picture of how the calcium sensing protein Synaptotagmin influences fusion phenotype, and how this influence may be used by chromaffin cells to tune their secretory response based on the degree of sympathetic nervous system (i.e. HSA axis) activation. When an organism is in a state of rest, HSA axis activity is minimal, meaning the splanchnic nerves will be releasing relatively small quantities of ACh and PACAP onto their postsynaptic chromaffin cells. As a result, the chromaffin cells will experience only mild rises in intracellular Ca^{2+}, which would favor exocytotic release from Syt-7-bearing LDCVs. These vesicular release events are predominantly characterized by a constricted fusion pore which likely limits the diffusion rate of cargo (i.e. biologically active signaling molecules such as epinephrine). Furthermore, many of these release events will end up undergoing endocytosis (i.e. kiss-and-run), which may serve as a way of conserving resources associated with vesicle biogenesis, packaging of cargo molecules, and clathrin-mediated retrieval of vesicle materials from the plasma membrane.

Conversely, when an organism is challenged by a stressor, HSA activity and splanchnic nerve output will increase dramatically, resulting in large Ca^{2+} spikes within chromaffin cells. In this context, secretion will occur from both Syt-7 and Syt-1 vesicles. The massive demands of this fight-or-flight scenario take priority over being stingy with vesicle materials and cargo, and therefore full-collapse fusion mediated by Syt-1 vesicles will be advantageous for the immediate need to, for example, upregulate heart rate and blood pressure (via Epi and NE) and increase pain tolerance (via enkephalins).

Preface to Thesis Research

Establishing the independent sorting and divergent secretory phenotypes of Syt-1 and Syt-7 in chromaffin cells was a major step in understanding the molecular regulation of exocytosis. However, these findings unveiled new questions regarding how Syt isoforms exert influence on the fusion mode of LDCVs. From a molecular standpoint, one of the most important questions is what domain(s) of Syt are responsible for their differential association with long-lived versus transient fusion pores. Considering their well-established role in binding Ca^{2+} and phospholipids, and the stark difference that Syt-1 and Syt-7 display in this respect, the Syt C2 domains arise as a primary candidate for regulating fusion pore dynamics.

Both the C2A and C2B domains of Syt are necessary for triggering exocytosis, however their respective roles appear to differ somewhat. For example, studies have suggested that Ca^{2+} binding to C2B plays a more important role in plasma membrane engagement and stabilization of fusion pores, whereas Ca^{2+} binding to C2A may act more like a permissive "switch" for exocytosis to occur (Tucker & Chapman, 2002; Bai & Chapman, 2004; Segovia *et al.*, 2010; Striegel *et al.*, 2012). Furthermore, a knockout study conducted in hippocampal neurons showed that replacing wild-type Syt-1 with a chimeric version containing the full Syt-7 C2B domain (in place of Syt-1 C2B) could not rescue the robust fast component of neurotransmitter release, suggesting that disparities between isoforms in this domain account for the phenotypic differences in fusion mode (Xue *et al.*, 2010).

As discussed above, the primary structures responsible for Ca^{2+} binding to Syt are the three flexible loops extending out from the top of each C2 domain β-sandwich (Fernandez-Chacon *et al.*, 2002). Figure 1.5 shows a comparison of the C2B domains of Syt-1 (A and D) and Syt-7 (B and E), illustrating that the C2B loops of Syt-7 can coordinate an additional Ca^{2+} ion.

Therefore, my research aimed to study the effects of mutating the Ca^{2+}-binding loops of the Syt-1 C2B domain to make them synonymous with the corresponding loops found in Syt-7. To this end, the phenotypic effects of individual loop conversions, as well as collective conversion of all three loops, were investigated by imaging individual exocytotic events associated with chimeric Syt-1:Syt-7 mutants. Based on the fusion mode preference of each isoform and the fact that mutations were performed in a Syt-1 background, phenotypically relevant loop conversions should be manifest as an increase in the persistence of fusion pores and possibly the chimeric Syt proteins themselves. The results of this study are described below.

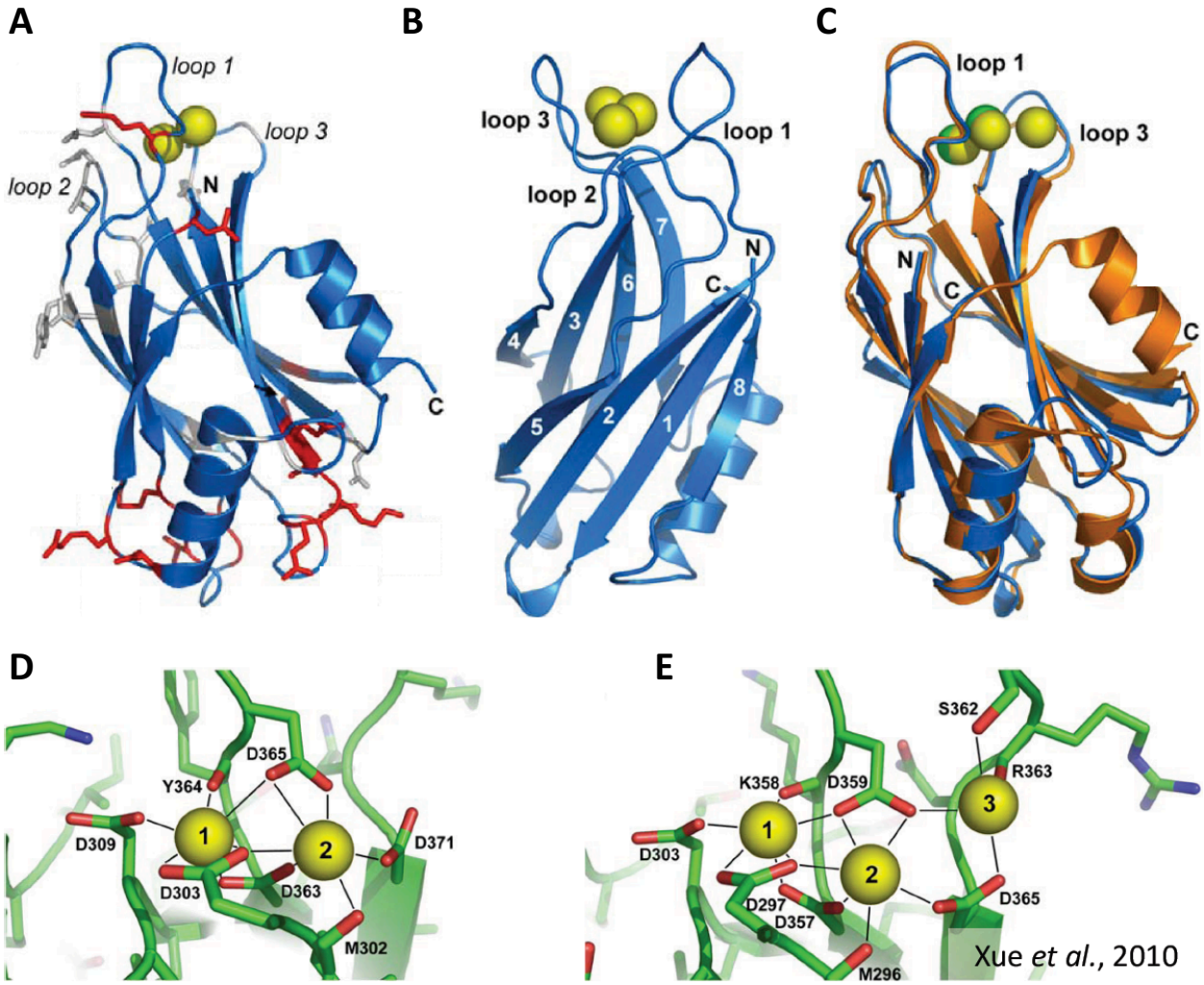

Figure 1.5: Comparison of Synaptotagmin C2B Domain Structures.
(A) Ribbon diagram of the Syt-1 C2B structure as determined by NMR spectroscopy with Ca^{2+}-binding loops labeled. **(B)** Syt-7 C2B domain structure as determined by X-ray crystallography with Ca^{2+}-binding loops labeled. **(C)** Overlay of Syt-1 (orange) and Syt-7 (blue) C2B structures from X-ray crystallography data. Ca^{2+} ions are depicted as yellow spheres. **(D and E)** Enlarged view of the Ca^{2+}-binding pocket of Syt-1 **(D)** and Syt-7 **(E)** based on X-ray crystallography. Amino acid residues implicated in Ca^{2+} binding are labeled and highlighted in red. Syt-7 residue numbers depicted in **(E)** are offset by -6 relative to the corresponding positions in Syt-1 due to differences in the upstream sequence. For example, M296 in (E) corresponds to M302 in (D). Note the additional Ca^{2+} ion bound by Syt-7. Figure reconstructed from Xue *et al.* 2010.

CHAPTER 2 – METHODS

Site-Directed Mutagenesis of Synaptotagmin-1 C2B Loops

Overall, the C2B domains of Syt-1 and Syt-7 are moderately similar in their amino acid sequence. However, this similarity is even more pronounced in the three Ca^{2+}-binding loops of the C2B domain (Figure 2.2 A). Therefore, site-directed mutagenesis was an appealing method for converting the Syt-1 C2B loops to match those of Syt-7.

To perform this mutagenesis, three sets of primers were designed, with each set containing a forward and reverse oligonucleotide that targeted a single C2B loop (Integrated DNA Technologies, Coralville, IA). These primers contained a central sequence matching the entire corresponding Syt-7 loop, flanked by 12-15 nucleotides homologous to the Syt-1 bases in the adjacent 5' and 3' regions outside of the loop (Figure 2.1; Table 2.1). Forward and reverse primers were designed to overlap in their binding to the complementary DNA strands containing the loop of interest. This allowed for the use of inverse polymerase chain reaction (PCR) to amplify the entire Syt-containing plasmid. Inverse PCR was carried out in a Bio-Rad T100 thermal cycler (Bio-Rad Laboratories, Hercules, CA) using CloneAmp HiFi PCR Premix (Clontech Laboratories, Mountain View, CA). The thermal cycler protocol included an initial heat activation step (98°C – 1 min) followed by 35 cycles of denaturation (98°C – 10 sec), annealing (55-58°C – 10 sec), and extension (72°C – 5 mins). After the last cycle, a final extension step was added (72°C – 5 mins) before the products were held at 4°C until further use. Wild-type Syt-pHluorin plasmid DNA used as a PCR template (and for control experiments) was a gift from Dr. Edwin R. Chapman (Department of Neuroscience, University of Wisconsin – Madison).

Figure 2.1: Site-Directed Mutagenesis Primer Design.
Binding sites for mutagenesis primers (purple) within the Syt-1 C2B domain (entire domain shown). Forward and backward primers were designed to completely overlap for inverse PCR. The DNA sequences of the C2B Ca^{2+}-binding loops are depicted in red.

Primer Name	Syt-1 Base Pair Range	Sequence (5'-3')
Syt1:7 $C2B_1$ Forward	880-939	CTGGAAGCCAAGAACCTCAAAGCCATGGACATCGGGGGCACATCAGACCCCTACGTGAAGATTCAC
Syt1:7 $C2B_1$ Reverse	880-939	GTGAATCTTCACGTAGGGGTCTGATGTGCCCCCGATGTCCATGGCTTTGAGGTTCTTGGCTTCCAG
Syt1:7 $C2B_2$ Forward	974-1026	GAAAAAGACGACGATTAAGAAGAGGAACCTGAATCCCTACTACAACGAGTCC
Syt1:7 $C2B_2$ Reverse	974-1026	GGACTCGTTGTAGTAGGGATTCAGGTTCCTCTTCTTAATCGTCGTCTTTTTC
Syt1:7 $C2B_3$ Forward	1071-1128	GTGGTAACTGTTTTGGACAAAGACAAGCTCAGCCGCAATGACGCCATCGGCAAAGTC
Syt1:7 $C2B_3$ Reverse	1071-1128	GACTTTGCCGATGGCGTCATTGCGGCTGAGCTTGTCTTTGTCCAAAACAGTTACCAC

Table 2.1: Site-Directed Mutagenesis Primer Sequences.
DNA sequences and specific Syt-1 base pair targets of all mutagenesis primers. The red portion of each primer sequence contains the mutagenic bases of the corresponding Syt-7 C2B loop, while the black portions correspond to the flanking C2B regions in Syt-1 used to "clamp" the primer to the Syt-1 template. The subscript number in the primer name indicates the C2B loop targeted by each primer set.

Inverse PCR products were digested with the methylation-specific endonuclease DpnI (New England Biolabs, Ipswich, MA). Due to its requirement for methylated DNA, DpnI will only

cleave template DNA present in the reaction mixture (in this case wild-type Syt-1), because this DNA has been previously replicated in *E. coli* containing the Dam methylase enzyme. Following DpnI digestion and heat inactivation, the remaining PCR products were transformed into competent DH5α cells according to the manufacturers recommendations, although with an additional two hours of incubation (Invitrogen Corporation, Carlsbad, CA). Six transformants were isolated from colonies grown overnight on Ampicillin-selective (Amp^+) agar media. Selected transformants were transferred to liquid Amp^+ media and again incubated overnight in a 37˚C shaker. The following day, DNA was isolated using the QIAprep Spin Miniprep Kit (Qiagen Company, Hilden, Germany), and after quantification the purified DNA was prepared for Sanger sequencing with primers targeting the Syt-1 C2B domain (Applied Genomics Technology Center, Wayne State University – School of Medicine, Detroit, MI).

DNA stocks containing the proper nucleotide substitutions were then subjected to a second round of Sanger sequencing with an array of primers designed to give a readout of the entire open reading frame containing the Syt-pHluorin fusion construct. This readout was compared to the wild-type Syt-1 construct sequence to ensure that mutagenesis was restricted to the desired C2B loop. Three single-loop Syt chimeras were generated: Syt1:7-$C2B_1$, Syt1:7-$C2B_2$, and Syt1:7-$C2B_3$ (subscript numbers corresponding to the C2B loop mutated in each construct). The resulting amino acid substitutions for each construct are as follows: *Syt1:7-$C2B_1$*: K301A, V304I, L307T; *Syt1:7-$C2B_2$*: N333R, T334N; *Syt1:7-$C2B_3$*: Y364K, I367L, G368S, K369R. The triple-loop chimera Syt1:7-$C2B_{1,2,3}$ contains all the above mutations and was generated by performing two additional rounds of mutagenesis; first, Syt1:7-$C2B_1$ was used as a template to mutate C2B loop 2, and then this product (Syt1:7-$C2B_{1,2}$) was used as the template in a second

reaction to mutate C2B loop 3. The full C2B amino acid sequences for these chimeras are depicted in Figure 2.2, A and B.

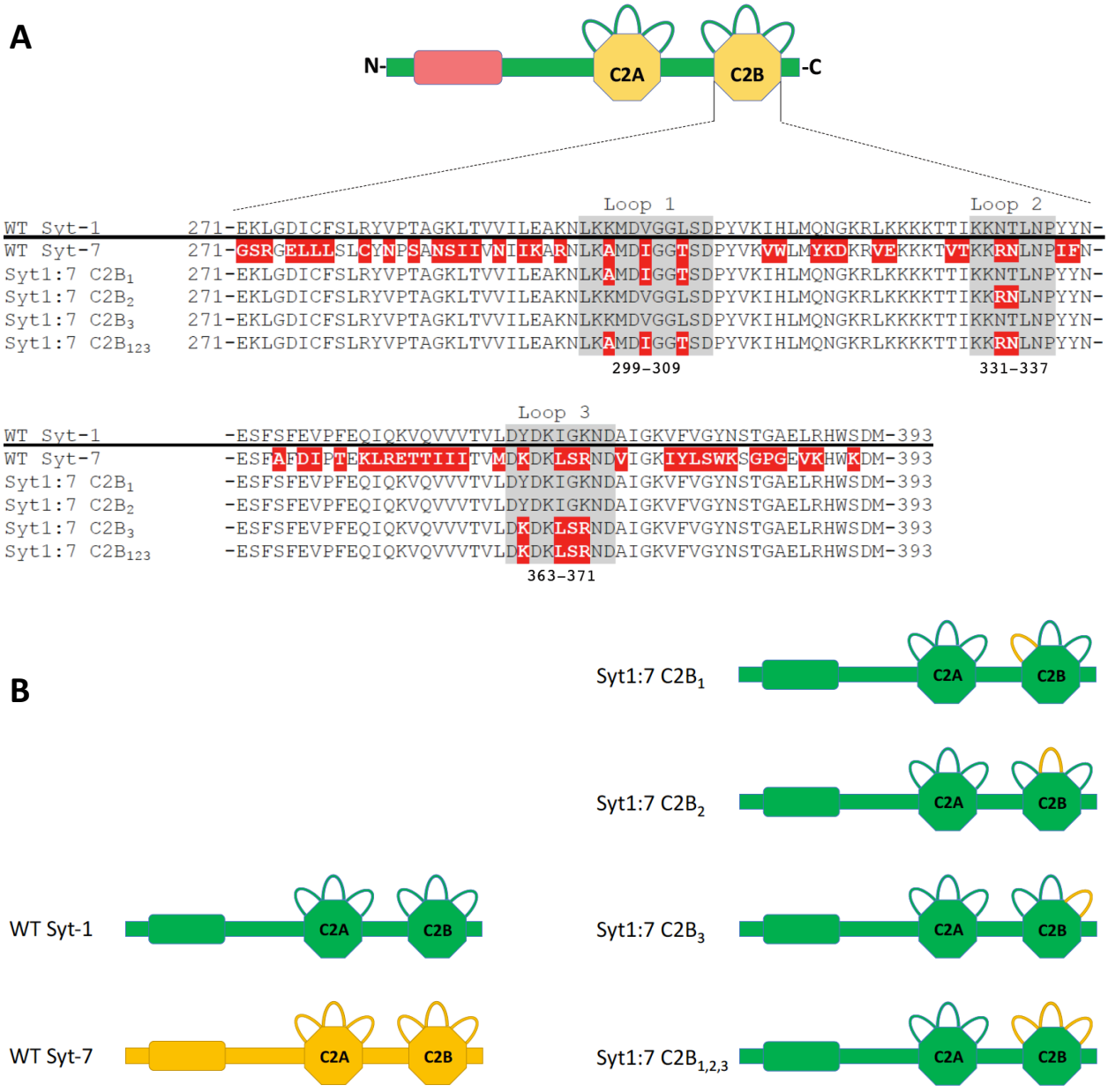

Figure 2.2: Synaptotagmin C2B Domain Alignments and Chimera Constructs.
(A) Alignment of the C2B domain amino acid sequences of Syt-1, Syt-7, and the four chimeric Syt constructs used in the current study. Amino acids highlighted in red indicate a deviation from the WT Syt-1 sequence. The gray shaded regions denote the Ca^{2+}-binding loops. Subscript numbers in the construct name indicate which C2B loop(s) has been mutated to match WT Syt-7. Amino

acid ranges based on the Syt-1 sequence are listed below each loop (see Figure 1.4 for all domain ranges). **(B)** Simplified depiction of the Syt1:7 chimeras illustrating the regions corresponding to either WT Syt-1 (green) or WT Syt-7 (yellow).

Isolation and Transfection of Bovine Chromaffin Cells

Adrenal glands of adult cows (*Bos taurus*) were obtained from JBS Packing Company (Plainwell, MI) on the day of slaughter and kept on ice during transit. The adrenal glands were cleaned in a non-divalent saline solution (145 mM NaCl, 5.6 mM KCl, 15 mM HEPES, 5.6 mM Glucose, 100 Units/ml Penicillin-Streptomycin), then injected with a pre-warmed mixture of 2:1 Liberase TH and TL (Sigma-Aldrich, St. Louis, MO) and placed in a beaker within a stationary incubator at 37°C. After 18 minutes, the glands were transferred to a clean beaker and the digestion was repeated with a fresh enzyme solution. Following this step, the glands were cut open and the medullary tissue was scraped off into a collection tube using a scalpel. The pooled tissue from all glands was minced by hand in a sterile pan with scalpels for 10 min, then incubated in a glass spinner flask with pre-warmed 2:1 Liberase TH and TL mixture at 37°C for 30 minutes. After incubation, the cell/tissue mixture was first rinsed through a 400 µm mesh screen using non-divalent saline solution and then centrifuged at 800 rpm to pellet chromaffin cells. Supernatant was discarded, and the procedure was repeated two more times with a 250 µm and 150 µm screen.

At this point, cells were resuspended in 1 ml of Buffer R from the Neon transfection kit (Thermo Fisher Scientific, Waltham, MA) and counted manually using a hemocytometer. Aliquots of suspended cells were made according to the manufacturer's recommendations and electroporated with 15 µg of the appropriate DNA construct via a single 1100 mV pulse applied for 40 milliseconds using the Neon transfection system (Thermo Fisher Scientific, Waltham, MA).

Electroporated cells were immediately plated on 35 mm glass-bottom dishes (refractive index 1.51; World Precision Instruments, Sarasota, FL) coated with poly-D-lysine and collagen at a density of 10^6 cells per dish. Dishes were pre-warmed with Dulbecco's Modified Eagle Medium: Nutrient Mixture F-12 (DMEM/F12) supplemented with 10% fetal bovine serum (Thermo Fisher Scientific, Waltham, MA) and a mixture of 100 Units/ml Penicillin-Streptomycin (Thermo Fisher Scientific, Waltham, MA) and 23.8 μg/ml Gentamicin (Sigma-Aldrich, St. Louis, MO). Plated cells were incubated in 5% CO_2 at 37°C for a minimum of 48 hours prior to imaging to ensure robust fusion protein expression. Experiments were completed within two days following this incubation time.

TIRF and pTIRF Microscopy

Background

Total Internal Reflection Fluorescence (TIRF) microscopy has been used in biological applications since the early 1980's (reviewed by Axelrod *et al.*, 1984). In theory, this microscopy method utilizes the physical property of light to reflect, rather than undergo refraction, when encountering an interface between two substances with different refractive indices (e.g. a glass coverslip and an aqueous biological sample). Importantly, this total internal reflection will only occur if the incoming light strikes the interface at or above a critical angle (θ_c) described by Snell's law:

$$\theta_c = \sin^{-1} (n_2/n_1)$$

In this equation, n_1 represents the refractive index of the first material that light will pass through (e.g. the glass coverslip), and n_2 is the index of the second material (e.g. a cell membrane). Although most light will be reflected back into the first material during TIRF (and

thus away from the sample), some of the incoming light will still propagate through to the second medium in the form of an “evanescent wave”. The advantage of TIRF microscopy is based on the fact that this evanescent wave decays exponentially as it enters the second material, meaning only objects relatively close to the sample interface (within ~100 nm) will be illuminated. This effectively increases image quality by eliminating background illumination of structures further into the sample. In the case of TIRF microscopy, the illuminating light source(s) are usually wavelength-specific lasers used to excite fluorophore-linked molecules within a cell (Figure 2.3).

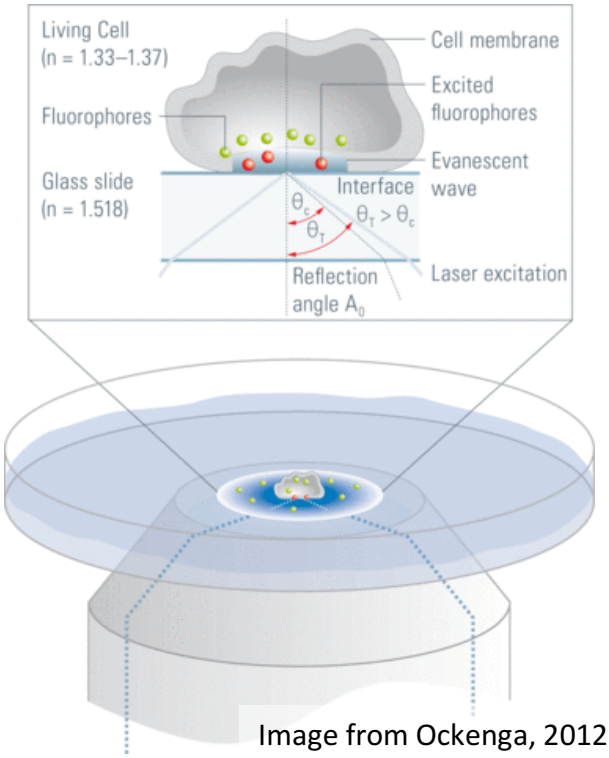

Image from Ockenga, 2012

Figure 2.3: Total Internal Reflection Fluorescence (TIRF) Microscopy.
The use of TIRF microscopy for imaging live cells in culture. One or more laser lines are guided into the objective of an inverted microscope at a TIRF angle (θ_T) greater than the critical angle (θ_c) described by Snell’s law relating the refractive indices of the glass coverslip and cell membrane (see text). This results in the propagation of an exponentially decaying “evanescent wave” into the cell that will selectively excite fluorophores near the coverslip (i.e. in the cell membrane or subplasmalemma). Image from Ockenga, 2012.

Over the years, TIRF microscopy has been adapted to meet various experimental needs, including the incorporation of polarized light sources (pTIRF) (Taraska & Almers, 2004; Anantharam *et al.*, 2010). Proper splitting and polarization of a laser results in one beam that specifically excites fluorophores oriented in the **s**ame plane as the coverslip-sample interface (***s***-polarlized; ***s***-pol), and another beam that excites fluorophores oriented **p**erpendicular to the interface (***p***-polarized; ***p***-pol). This setup is advantageous for imaging topological changes in the plasma membrane using membrane-intercalating dyes (e.g. DiD, DiI), because their transition dipole moment (i.e. the plane they can be excited in) is roughly parallel to the membrane surface they sit within (Axelrod, 1979). Therefore, during an exocytotic event, the *s*-pol beam will primarily excite dye in the plasma membrane surrounding a fusion pore, whereas the *p*-pol beam will excite dye in the "walls" of a secretory vesicle and fusion pore (Figure 2.4, A and B).

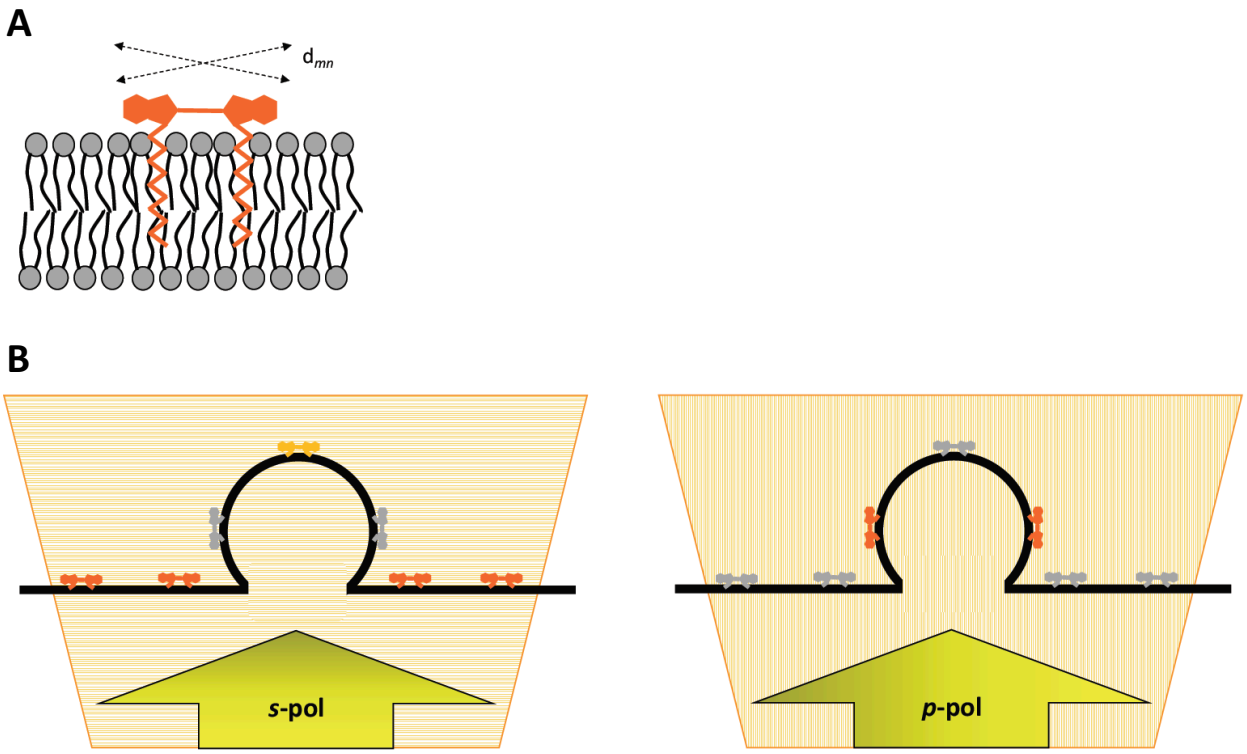

Figure 2.4: Visualizing Membrane Topology with Membrane-Intercalating DiD.
(A) Orientation of a DiD molecule intercalated into a lipid bilayer. Membrane insertion is mediated by two long, lipophilic hydrocarbon chains. The resulting absorption and emission transition dipole moments (d_{mn}) are therefore roughly parallel to the surface of the membrane the molecule is residing within. **(B)** The orientation of DiD can be exploited to track membrane topology by using a polarized excitation light source. 561-nm *s*-polarized light (*s*-pol) will primarily excite DiD in the plasma membrane parallel to the glass coverslip, with a small contribution from dye marking the back of fused vesicles (because these molecules are much deeper in the evanescent field; *left image*). Conversely, *p*-polarized light (*p*-pol) will selectively excite DiD oriented perpendicular to the coverslip in membrane forming the walls of a fused vesicle (orange molecules, *right image*).

Using the emission intensity values elicited from *s*- and *p*-pol excitation, two meaningful parameters can be computed. The P/S intensity ratio at a fusion site reports on the degree of membrane curvature. A higher ratio indicates that more of the stained membrane is oriented perpendicular to the plasma membrane surface, and is therefore characteristic of vesicles that are at the point of having merged with the plasma membrane and formed a fusion pore. When this vesicle eventually undergoes full-collapse, or conversely reseals and undergoes endocytosis (kiss-and-run), the ratio will drop back down closer to its pre-fusion value as the plasma membrane flattens and the vesicle leaves the evanescent field. A second parameter, the P+2S value, has been shown in previous studies to correspond with the total amount of dye in a region but is also influenced by how deep the dye molecules are in relation to the evanescent field (Anantharam *et al.*, 2010; 2012). At least in theory, an increase in P+2S values during exocytosis could correspond to a vesicle that is connected to the plasma membrane by a narrow fusion pore, as this would serve as an accumulation point for dye near the coverslip (where the evanescent field is strongest). A decrease in P+2S could therefore result from dye diffusing into a depression formed by the membrane of a collapsing vesicle and thus moving further away from the coverslip.

Experimental pTIRF Wavelengths and Fluorophores

The thesis research presented here was conducted using the same pTIRF microscopy system as Rao *et al.* (2014). This system employs two solid-state lasers (Coherent Inc., Santa Clara, CA); a 488-nm laser used to excite the Synaptotagmin-linked fluorescent protein pHluorin (described below), and a 561-nm laser whose output is split into two orthogonally polarized beams used to selectively excite the membrane-intercalating dye DiD (Invitrogen Corporation, Carlsbad, CA) based on its orientation (see above). The current study focused primarily on the persistence of topological changes (i.e. elevated P/S ratios) and pHluorin signatures following membrane fusion mediated by Syt chimeras.

The fluorescent protein pHluorin (pHl) was used for the current study, because its pH sensitivity serves as a conspicuous indicator of exocytotic events. pHl was developed from Green Fluorescent Protein (GFP), and shows maximal fluorescence emission between pH values of 7.0-8.0, while being almost entirely quenched in more acidic environments (pH ~5.5) (Miesenbock *et al.*, 1998). These pH values coincide closely with the conditions in living chromaffin cells, where the internal pH of large dense-core vesicles (LDCVs) is maintained at ~5.5 by vesicular ATPases, while the surrounding extracellular environment is more neutral at ~7.4. Based on these features and the vesicular localization of Synaptotagmin, this study used a fusion protein with pHl attached to the N-terminus of Syt, thus confining the fluorophore within the acidic vesicle lumen prior to exocytosis (Figure 2.5).

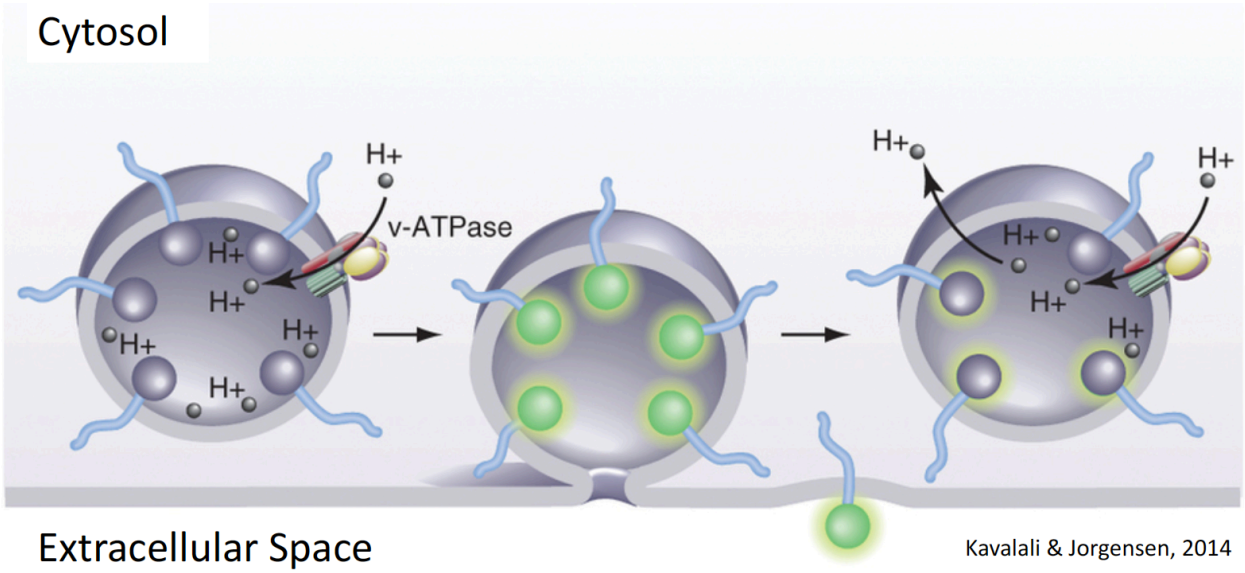

Figure 2.5: Visualizing Exocytosis with pH-Sensitive pHluorin.
Left: Prior to exocytosis, pHluorin (pHl) fluorescence is quenched due to the acidity of the vesicle lumen (pH ~5.5) maintained by vesicular-ATPases. *Center:* Upon fusion, the formation of a fusion pore results in rapid neutralization of the lumen and a concomitant increase in pHluorin fluorescence. *Right:* pHl in vesicles that are endocytosed via kiss-and-run will again be quenched as the vesicle lumen is re-acidified. Image reproduced from Kavalali & Jorgensen, 2014.

Using this setup, docked vesicles awaiting exocytosis emit little-to-no fluorescence when exposed to the 488-nm laser. However, once exocytosis begins and a fusion pore opens between the vesicle lumen and extracellular fluid, the luminal pH rapidly neutralizes, causing pHl molecules exposed to 488-nm light to fluoresce brightly. This fluorescence will persist at the fusion site until one of two outcomes occur; either (1) the vesicle collapses into the plasma membrane (i.e. classic exocytosis) and the Syt-pHl molecules diffuse away from the fusion site, or (2) the fusion pore reseals, and the vesicle undergoes endocytosis (i.e. kiss-and-run) following which it will re-acidify (thereby quenching the fluorescence once again).

Image Acquisition

The three incoming laser lines (488-nm, *s*-pol 561-nm, *p*-pol 561-nm) were aligned in a single 60x (1.49 numerical aperture) objective on an Olympus IX81 inverted microscope (Olympus Corporation, Center Valley, PA). Illumination of the sample was achieved using rapid cycling of Lambda SC shutters (Sutter Instruments, Novato, CA) to sequentially allow the transmission of a single beam onto the sample. Output emission was captured using an Andor iXon EMCCD Ultra 897 camera (Andor Technology, Concord, MA) controlled by MetaMorph imaging software (Molecular Devices, Sunnyvale, CA). Collectively, this setup allowed for image acquisition at ~2.5 frames per second for each channel, and produced a total optical magnification of ~200x, which translated into a pixel size of ~80 nm in the analyzed images.

Live Imaging of Chromaffin Cells

Prior to imaging, media was removed and culture plates containing chromaffin cells were washed three times with a basal saline solution (basal PSS) containing: 145 mM NaCl, 5.6 mM KCl, 2.2 mM $CaCl_2$, 0.5 mM $MgCl_2$, 5.6 mM glucose, 15 mM HEPES, pH 7.4. Cell membranes were then labelled by adding 10 µl of DiD to 2 ml of basal PSS and swirling this solution on the plate for ~15-20 sec at room temperature. Following this step, the dye solution was poured off and plates were washed three more times to remove excess dye. Individual cells were selected for imaging if they showed both DiD staining and pHluorin expression (though this was usually very weak prior to cell stimulation). During imaging, plates were bathed in basal PSS and the targeted cell was selectively stimulated using solutions administered through a perfusion needle (100 µm inner diameter; ALA Scientific Instruments, Westbury, NY) positioned just outside the field of view using a micromanipulator. Cells were perfused sequentially with 5 sec of basal PSS, 75 sec of elevated K^+ (56 mM KCl) PSS to trigger exocytosis, and 10 sec of basal PSS again to clear the

stimulating solution from the perfusion needle. The elevated K^+ PSS solution contained: 95 mM NaCl, 56 mM KCl, 5 mM $CaCl_2$, 0.5 mM $MgCl_2$, 5.6 mM Glucose, 15 mM HEPES, pH 7.4. Perfusion times were regulated via software coupled to electromagnetic valves (ALA Scientific Instruments, Westbury, NY) and synchronized with the start of image acquisition. Experiments were carried out under ambient air conditions, with the temperature typically ranging between 24-26 °C in the imaging room.

Image Analysis

Acquired image stacks for each channel (488-nm, *s*-pol 561-nm, *p*-pol 561-nm) were first processed using a custom IDL software script written by Daniel Axelrod (Department of Physics, University of Michigan – Ann Arbor). This software performs three important functions: (1) It spatially aligns the images captured from all channels at each time point for a given cell, thereby allowing the user to select a ~270 nm region of interest (ROI) around single fusion events across all channels at once. (2) It normalizes the *p*-pol and *s*-pol image stacks against Rhodamine 6G images taken by the user on the same microscope setup (see below). (3) The software generates composite images of the pixel-by-pixel *p*/*s* intensity ratios and *p*+2*s* values across the cell for each time point. Normalization of *p*- and *s*-pol images uses a Rhodamine 6G solution (Sigma-Aldrich, St. Louis, MO), which is assumed to have randomly oriented transition dipole moments. This is an important step for factoring out orientation biases imposed by the optical setup, and essentially corrects for small differences in the intensity of the incoming laser beams that could otherwise skew the P/S ratio.

For each cell analyzed, the final output from the IDL software is a series of text documents with the averaged (across the ROI) fluorescence intensity at every time point during image

acquisition. A separate document is created for the pHl emission intensities, P/S ratios, and P+2S values in each ROI, and this is done for all ROIs selected within a given cell. These values were then transferred to an excel document and graphed. Exocytotic events (i.e. ROIs) were only included in the analysis if they showed a significant change (>10%) in all three values within five frames (~2 sec) of the fusion frame, as indicated by the spike in pHl emission intensity. As expected, pHl and P/S ratio values always increased following fusion, whereas P+2S values either increased or decreased. The 10% significance threshold used in this study was based on a similar (albeit slightly less stringent) threshold of 7% used by Rao *et al.* (2014), and this change was measured in relation to the average parameter value in the three frames prior to fusion (i.e. the pre-fusion baseline). All reported durations reflect the amount of time a given parameter remained above this 10% threshold following the initial rise. The number of cells and total number of events across all cells for each construct are reported in Table 2.2.

Construct	# of Cells	# of Events (Total)
WT Syt-1	5	41
WT Syt-7	6	68
Syt1:7-C2B$_1$	5	42
Syt1:7-C2B$_2$	11	73
Syt1:7-C2B$_3$	6	87
Syt1:7-C2B$_{1,2,3}$	5	61

Table 2.2: Number of Cells and Fusion Events Analyzed.
Events were selected based on the criteria described above. For a given cell, events were included in the analysis if the fluorescence signal of pHl, P/S, and P+2S changed by at least 10% (relative to the pre-fusion baseline) within five frames of the spike in pHl indicating vesicle fusion. The number of events reported in the table reflects how many total events for each construct were pooled together in the quantitative analysis based on meeting this criterion.

CHAPTER 3 – RESULTS AND DISCUSSION

Results

The Post-Fusion Persistence of Chimeric Synaptotagmins Differs from Wild-Type

The spatial and temporal dynamics of fusion machinery proteins can differ substantially, providing clues to their respective roles in the fusion process. For instance, Rao *et al.* (2014) compared the post-fusion persistence of pHluorin-tagged Synaptotagmin (Syt) isoforms at sites of exocytosis. In the current study, this was initially investigated for control data (i.e. wild-type [WT] Syt-1 and Syt-7) to validate the previously published findings on the behavior of these isoforms. It was found that WT Syt-7 pHl remained punctate at sites of exocytosis for tens of seconds, whereas WT Syt-1 pHl signal was rapidly lost (Figure 3.1). Plotting the durations of numerous individual fusion events across multiple cells revealed a highly divergent trend, where 87% of Syt-7 events were characterized by persistent aggregation of the protein at the fusion site for more than 20 sec compared to only 27% of Syt-1 events suggesting different functions for these isoforms (Figure 3.2, A-C).

χ^2 Comparison	Test Statistic	*p*-value	df
WT Syt-1 vs. WT Syt-7	46.39	< 0.00001	2
WT Syt-1 vs. Syt1:7-C2B$_1$	-	-	-
WT Syt-1 vs. Syt1:7-C2B$_2$	3.48	0.17552	2
WT Syt-1 vs. Syt1:7-C2B$_3$	2.02	0.36422	2
WT Syt-1 vs. Syt1:7-C2B$_{1,2,3}$	15.97	0.00034	2

Table 3.1: Chi-Square Analysis of Protein Persistence.
Pairwise Chi-Square tests for homogeneity were used to assess whether protein persistence distributions differed significantly between Syt constructs. All individual events for each construct were binned into three groups based on how long the pHluorin signal remained elevated

following fusion (0-20 sec, 20-40 sec, or >40 sec). The distributions of WT Syt-7 and chimera Syt1:7 $C2B_{1,2,3}$ differed significantly from WT Syt-1, whereas Syt1:7 $C2B_2$ and Syt1:7 $C2B_3$ did not. This analysis could not be performed on Syt1:7 $C2B_1$, because the data for this comparison did not meet the second of the two required assumptions for a Chi-Square test (all expected values ≥1 and no more than 20% of expected values <5).

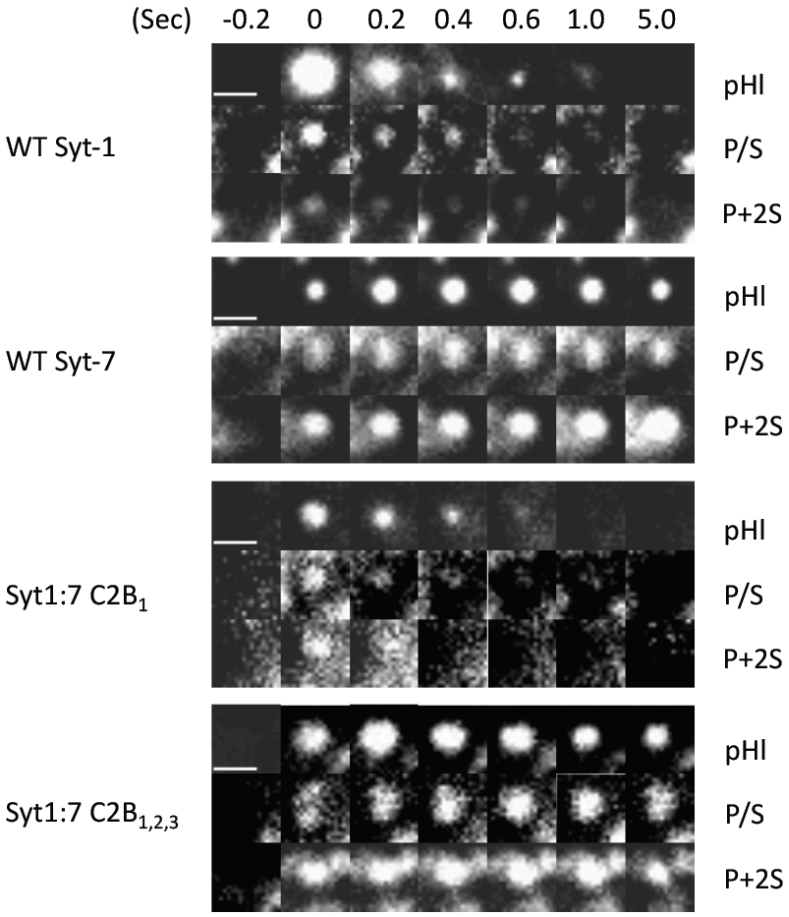

Figure 3.1: Sample Image Sequences of Synaptotagmin Constructs.
Sample time-lapse image sequences of individual fusion events from the indicated Syt constructs. The top row for each construct shows the pHluorin emission used to determine the time of vesicle fusion (t= 0 sec) and track protein persistence. The middle row (P/S) and bottom row (P+2S) report on the pixel-by-pixel membrane curvature and DiD concentration, respectively. Note the elevated persistence of Syt1:7 $C2B_{1,2,3}$ protein and membrane curvature in comparison to WT Syt-1. Scale bar, 800 nm.

To identify what portion of the Syt-isoforms contributed to these differences, the chimeras were tested in this assay and compared to the wild-type isoforms. It was found that the single loop Syt chimeras, Syt1:7-$C2B_1$, Syt1:7-$C2B_2$, and Syt1:7-$C2B_3$ all showed a less

dichotomous trend, with protein persisting for >20 sec in 33%, 38%, and 39% of events, respectively (Figure 3.2 C). Binning of persistence durations for all events into three groups (<20 sec, 20-40 sec, >40 sec) enabled the comparison of each chimeric distribution with WT Syt-1 (Table 3.1). Although this comparison did not show significance at the $\alpha = 0.05$ significance level, it was evident from plotting all durations that these chimeras generally exhibited an intermediate phenotype, with more balance between events showing persistence versus rapid loss of protein (Figure 3.2 A). This is more clearly observed by comparing the average time of persistence for the middle 50% of durations (i.e. durations within the inner quartile range, IQR). Performing this calculation, Syt-1 had an average persistence of 10.8 sec (SEM ± 1.14 sec), while Syt-7 averaged 56.2 sec (SEM ± 2.04 sec). All three single loop chimeras showed a modest increase in this value from their Syt-1 source DNA, with averages of 13.4 sec (SEM ± 1.16 sec), 14.2 sec (SEM ± 1.65 sec), and 16.4 sec (SEM ± 0.93 sec), respectively (Figure 3.2 B; Table 3.2). This suggests that single C2B loop conversions between Syt-1 and Syt-7 have a small but noticeable effect on persistence of the protein at fusion sites.

Construct	Avg. Protein Persistence of Events within IQR (sec)
WT Syt-1	10.8 ± 1.14
WT Syt-7	56.2 ± 2.04
Syt1:7-C2B$_1$	13.4 ± 1.16
Syt1:7-C2B$_2$	14.2 ± 1.65
Syt1:7-C2B$_3$	16.4 ± 0.93
Syt1:7-C2B$_{1,2,3}$	31.2 ± 2.76

Table 3.2: Average Protein Persistence Following Fusion.
Values indicate the average duration (and SEM) of elevated pHluorin signal (>10% of the pre-fusion baseline) for events that fell within the inner quartile range (see Figure 3.2 B).

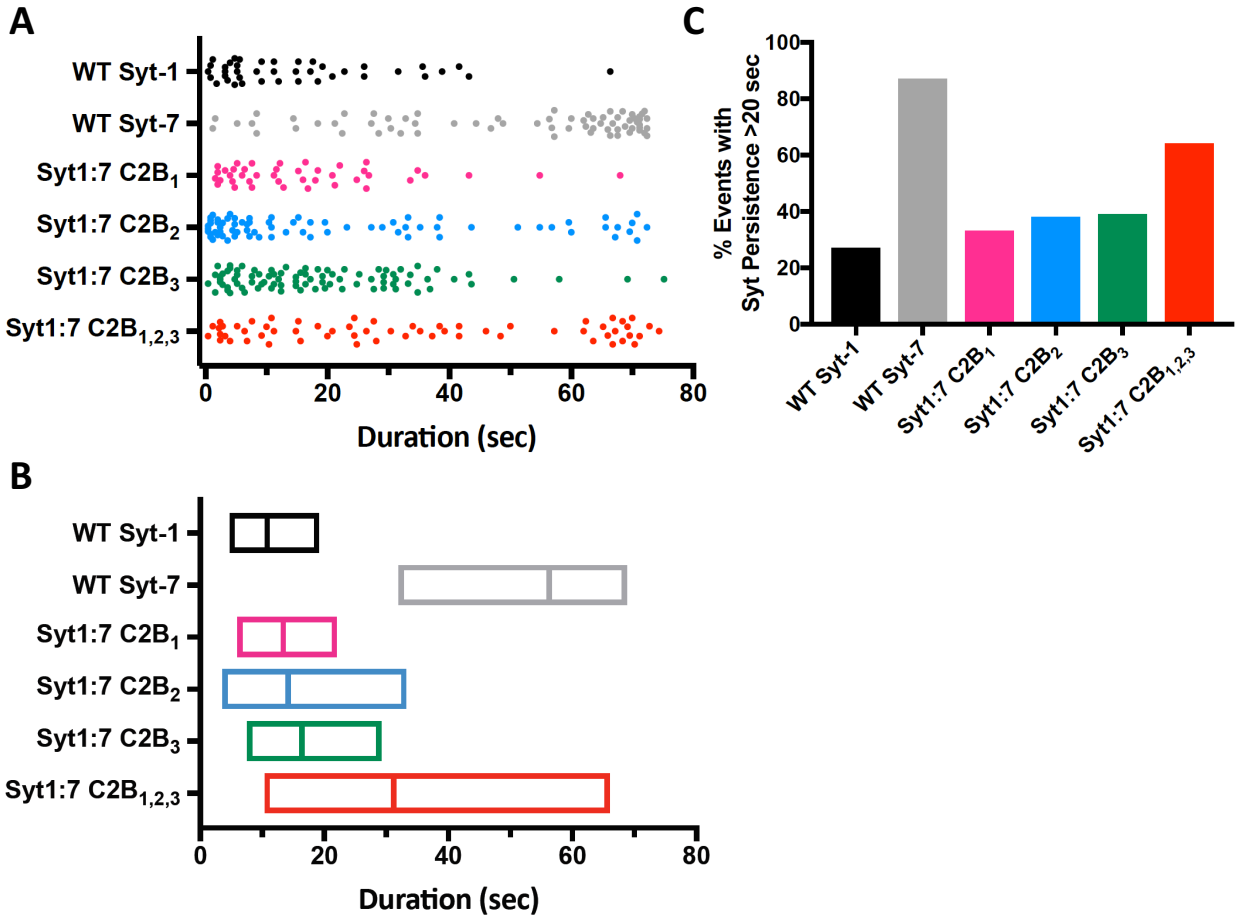

Figure 3.2: Persistence of Synaptotagmin Chimeras at Fusion Sites.
(A) Scatter dot plots of protein persistence for all individual fusion events based on pHluorin emission profiles. Durations indicate the amount of time the pHl signal remained above the 10% threshold following its initial rise at the time of fusion. As described in the text, some of the higher values reflect truncated durations due to the end of image acquisition occurring before the signal dropped below the 10% threshold. Note the cluster of long-duration events for chimera Syt1:7 $C2B_{1,2,3}$ in comparison to WT Syt-1. **(B)** Box plots depicting the inner quartile range (IQR) of durations and the average duration computed from all events within the IQR. **(C)** Graph reporting the percentage of all events for each construct that showed protein persistence in excess of 20 sec based on the pHl fluorescence signal. Again, note the intermediate phenotype of Syt1:7 $C2B_{1,2,3}$.

Synaptotagmin Ca^{2+}-binding Loops Also Influence Fusion Pore Expansion

In addition to tracking the persistence of the Syt chimeras at fusion sites, polarized total internal reflection fluorescence (pTIRF) microscopy was used to investigate the behavior of the

vesicular and plasma membranes following initial fusion. Using this system, topological changes indicative of a vesicle fusing with the plasma membrane are reported as a sharp rise in the P/S fluorescence ratio (see methods). This value remains elevated until either (1) the fusion pore dilates and the vesicle membrane flattens into the plasma membrane (i.e. full-collapse fusion), or (2) the fusion pore reseals (i.e. kiss-and-run endocytosis) and the vesicle is brought out of the evanescent field.

Consistent with Rao *et al.* (2014), this study found that in control cells, elevated P/S ratios persisted far longer for WT Syt-7-mediated exocytotic events than for WT Syt-1 events. Given that the Syt chimeras were generated in a Syt-1 background (Figure 2.2), functionally relevant loop swaps were expected to result in fusion events where P/S remained elevated longer than for WT Syt-1. Interestingly, all single loop chimeras showed an increase in the average duration of elevated P/S ratios (Figure 3.3, A and B). However, the finite imaging time and variation in when events occurred following cell stimulation led to some of the longer duration values being truncated (i.e. because the elevated P/S ratio persisted beyond the end of the image acquisition period). Therefore, it is more reliable to calculate average times for each construct based only on values within the inner quartile range (IQR). Chimeras Syt1:7-C2B$_1$ and Syt1:7-C2B$_2$ showed only a modest increase in elevated P/S duration from 7.3 sec (SEM ± 0.94 sec) for WT Syt-1 to 13.9 sec (SEM ± 2.91 sec) and 15.3 sec (SEM ± 1.63 sec), respectively. On the other hand, swapping of C2B loop 3 (chimera Syt1:7-C2B$_3$) appeared to have a more substantial influence on prolonging the decay of P/S ratios, with an average duration of 27.6 sec (SEM ± 2 sec) compared to 38.6 sec (SEM ± 2.74 sec) for WT Syt-7 (Figure 3.3 B; Table 3.4). Using Chi-Square analysis to compare all P/S

durations for each chimera against WT Syt-1 revealed that the difference between the distribution of Syt1:7-C2B$_3$ and WT Syt-1 was highly significant ($p < 0.001$; Table 3.3).

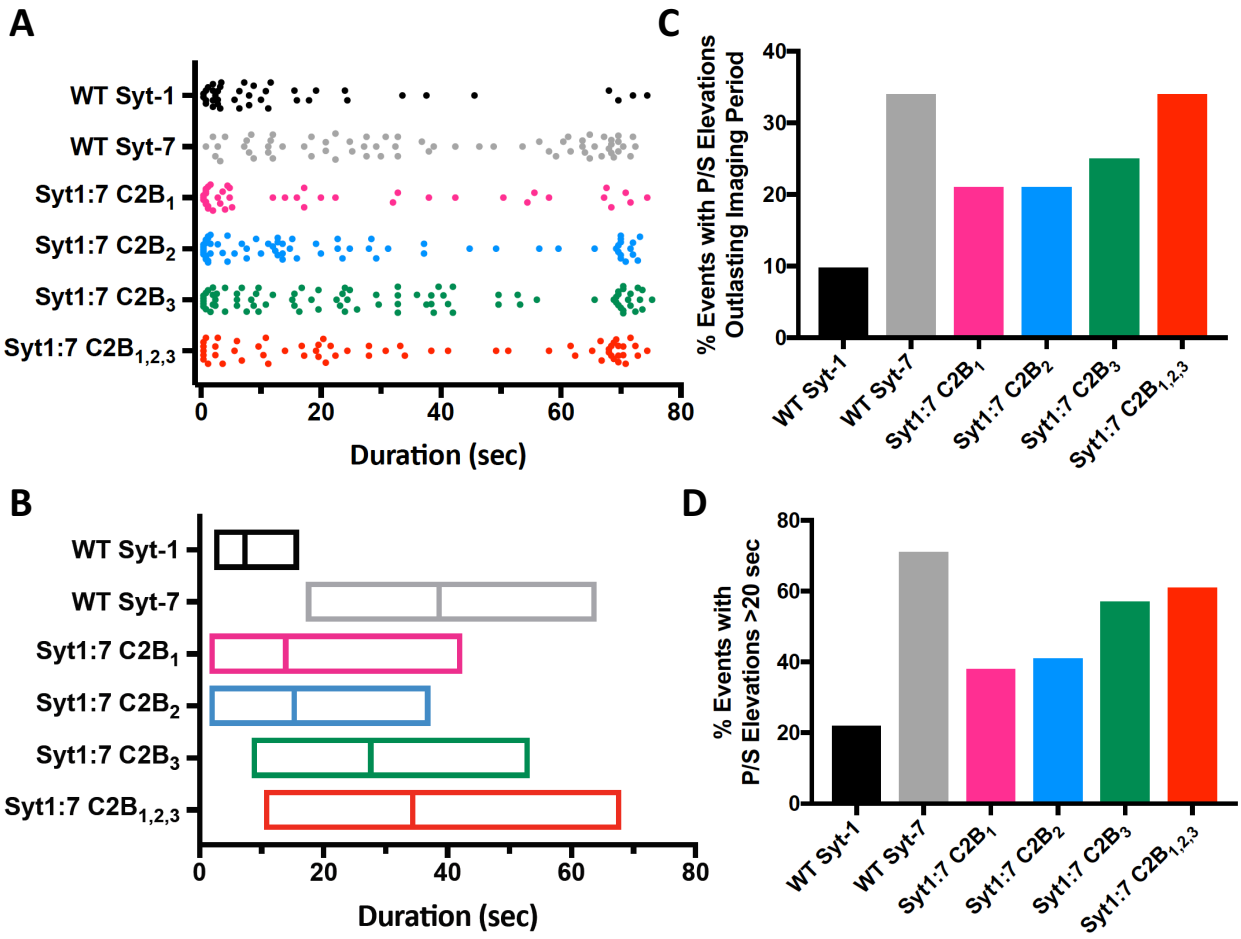

Figure 3.3: Post-Fusion Elevations in P/S Ratio.
(A) Scatter dot plots of the elevated P/S ratio duration for all individual fusion events. Durations indicate the amount of time the P/S ratio in an ROI remained above the 10% threshold following its initial rise at the time of fusion. As described in the text, some of the higher values reflect truncated durations due the end of image acquisition (see panel **C**). Note the clusters of long-duration events for chimeras Syt1:7 C2B$_2$, Syt1:7 C2B$_3$, and Syt1:7 C2B$_{1,2,3}$ in comparison to WT Syt-1. **(B)** Box plots depicting the inner quartile range (IQR) of elevated P/S durations and the average duration computed from all events within the IQR. **(C)** Graph indicating the percentage of all events for each construct in which P/S remained elevated beyond the end of the image acquisition period. Syt1:7 C2B$_{1,2,3}$ was indistinguishable from WT Syt-7 in this respect. **(D)** Graph reporting the percentage of all events that showed elevated P/S ratio durations in excess of 20 sec based on DiD emission.

χ^2 Comparison	Test Statistic	*p*-value	df
WT Syt-1 vs. WT Syt-7	24.34	< 0.00001	2
WT Syt-1 vs. Syt1:7-C2B$_1$	-	-	-
WT Syt-1 vs. Syt1:7-C2B$_2$	4.41	0.11025	2
WT Syt-1 vs. Syt1:7-C2B$_3$	14.19	0.00083	2
WT Syt-1 vs. Syt1:7-C2B$_{1,2,3}$	15.30	0.00048	2

Table 3.3: Chi-Square Analysis of Elevated P/S Durations.
Pairwise Chi-Square tests for homogeneity were used to compare the distributions of elevated P/S ratios between Syt constructs. All individual events for each construct were binned into three groups based on how long the P/S ratio remained elevated following fusion (0-20 sec, 20-40 sec, or >40 sec). The distributions of WT Syt-7, Syt1:7 C2B$_3$, and Syt1:7 C2B$_{1,2,3}$ differed significantly from WT Syt-1. This analysis could not be performed on Syt1:7 C2B$_1$, because the data for this comparison did not meet the second of the two required assumptions for a Chi-Square test (all expected values ≥1 and no more than 20% of expected values <5).

Elevations in P/S outlasted the imaging period more frequently for Syt-7 events (~34%) than for Syt-1 (<10%) (Figure 3.3 C). Chimera Syt1:7-C2B$_3$ events behaved more like Syt-7 in this regard, with ~25% of all analyzed events persisting beyond the end of acquisition. Binning events based on a 20-sec threshold revealed a similar trend. For chimera Syt1:7-C2B$_3$, 50 out of 87 events (~57%) exhibited a P/S signal lasting longer than 20 sec, which resembled the case of WT Syt-7 (~71%) more than WT Syt-1 (22%) (Figure 3.3 D). Unexpectedly, P+2S values (reporting on overall dye concentration at the fusion site) showed a post-fusion increase (versus a decrease) for nearly all events across constructs. This ranged from 88% of WT Syt-1 events to 97% of WT Syt-7, with all chimeric proteins falling in the middle at ~95% (data not shown). This will be discussed in greater detail below. Overall, these findings suggest that the Syt-7 C2B loops can individually impede the expansion of the exocytotic fusion pore, with the most significant impact on this behavior resulting from loop 3.

Construct	Avg. P/S Elevation of Events within IQR (sec)
WT Syt-1	7.3 ± 0.94
WT Syt-7	38.6 ± 2.74
Syt1:7-C2B$_1$	13.9 ± 2.91
Syt1:7-C2B$_2$	15.3 ± 1.63
Syt1:7-C2B$_3$	27.6 ± 2
Syt1:7-C2B$_{1,2,3}$	34.4 ± 3.56

Table 3.4: Average Duration of Elevated P/S Ratios Following Fusion.
Values indicate the average duration (and SEM) of elevated P/S ratios (>10% of the pre-fusion baseline) for events that fell within the inner quartile range (see Figure 3.3 B).

Chimera Syt1:7-C2B$_{1,2,3}$ Behaves the most like Wild-Type Syt-7

The fact that individual C2B loop swaps appeared to influence exocytosis raised the question of whether swapping all three loops together would further push the secretory behavior of Syt-1 towards that of Syt-7. This was addressed by analyzing the phenotype of the triple loop mutant Syt1:7-C2B$_{1,2,3}$, in which all three Ca^{2+}-binding loops in Syt-1 C2B were replaced with those of Syt-7. The typical behavior of this protein in relation to WT Syts and the loop 1 mutant can be seen in the sample time-lapse images shown in Figure 3.1. Regarding protein persistence following fusion, the single loop chimeras did not strongly favor a single phenotype (i.e. persistence or rapid diffusion), whereas Syt1:7-C2B$_{1,2,3}$ was more reminiscent of WT Syt-7, with ~64% of events characterized by persistence exceeding 20 sec (Figure 3.2, A and C). The average residence time for the middle 50% of durations, 31.2 sec (SEM ± 2.76 sec), was also shifted further from WT Syt-1 than the single loop chimeras (Figure 3.2 B; Table 3.2).

Furthermore, the triple loop chimera had the greatest influence on post-fusion membrane topology. Events that fell within the IQR had an average P/S rise that lasted for 36 sec (SEM ± 3.56 sec), nearly as long as WT Syt-7 (38.3 ± 2.99 sec) (Figure 3.3, A and B; Table 3.4). Likewise, more than 60% of Syt1:7-C2B$_{1,2,3}$ events showed a P/S elevation exceeding 20 sec (compare to above), with ~34% of all elevations outlasting the imaging period (roughly the same as for WT Syt-7; Figure 3.3, C and D). The duration distributions for persistence of both protein and membrane topology were highly significant between Syt1:7-C2B$_{1,2,3}$ and WT Syt-1 ($p < 0.0005$; Tables 3.1 and 3.3). Taken together, these results suggest that the amino acids within the Syt C2B Ca^{2+}-binding loops influence both the persistence of Syt at fusion sites and the post-fusion expansion of the exocytotic fusion pore. Furthermore, the effects of swapping in all three Syt-7 C2B loops together are more pronounced than that of any individual loop swap.

Discussion

This study focused on the molecular basis for the previously observed differences in the behavior of Syt-1 and Syt-7 in adrenal chromaffin cells. To this effect, chimeric proteins were generated in which the Ca^{2+}-binding loops in the Syt-1 C2B domain were replaced by loops from the same region in Syt-7. The data presented above suggest that the genetic makeup of these loops influences at least two of the differential properties between isoforms during exocytosis; namely, the persistence of the Syt protein and the behavior of the fusion pore. All chimeras showed at least a slight shift from the Syt-1 phenotype towards that of Syt-7, with the triple loop mutant (Syt1:7-C2B$_{1,2,3}$) behaving most like Syt-7. The effects of single loop swaps did not appear to be strictly additive when compared to the triple loop mutant, and this may reflect the fact that C2 domain Ca^{2+} binding results from the coordinated arrangement of multiple loops to form a

Ca^{2+}-binding pocket, rather than each loop interacting with independent Ca^{2+} ions (Figure 1.5; Shao *et al.*, 1996; Sudhof & Rizo, 1996).

In addition to the findings of Rao *et al.* (2014), increased persistence and aggregation of Syt-7 following fusion was confirmed more recently using the super-resolution method of Stochastic Optical Reconstruction Microscopy (STORM; Rao, 2016). The findings presented here suggest that Ca^{2+}-mediated binding specifically by the C2B domain influences how long Syt remains clustered at sites of exocytosis. This clustering may result from Syt interacting with phospholipids in the membrane, other fusion machinery proteins, and/or forming homo-oligomers with itself. It was recently demonstrated *in vitro* that the cytosolic fragment of Syt-7 (containing C2A and C2B) dissociates from liposomes containing negatively-charged phosphatidylserine (PS) far more slowly than Syt-1 when Ca^{2+} is chelated out of the system (Rao, 2016). Therefore, it is reasonable to predict that conversion of the Syt-1 C2B loops would slow the rate of membrane release, which is consistent with what was observed regarding diffusion of the Syt1:7 chimeras. Syt1:7-$C2B_{1,2,3}$ showed the most pronounced reduction in diffusion, remaining punctate for roughly 20 sec longer than WT Syt-1 on average (Figure 3.2; Table 3.2).

Tracking membrane topology using pTIRF revealed a similarly striking trend. P/S ratios remained elevated far longer following fusion events mediated by Syt1:7-$C2B_3$ and Syt1:7-$C2B_{1,2,3}$ than WT Syt-1 (Figure 3.3; Tables 3.3 and 3.4). As mentioned above, P/S ratios increase as a result of DiD reorientation during vesicle and plasma membrane fusion. A subsequent decrease in P/S would in theory occur due to one of two contrasting outcomes; either fusion pore dilation and concomitant vesicle collapse, or fusion pore closure (endocytosis) followed by trafficking of the vesicle out of the evanescent field. This suggests that in the case of the Syt1:7 chimeras, fusion

pores were either more often delayed in their expansion, or they tended to reseal, with the vesicle remaining in close apposition to the plasma membrane. In other words, the C2B loops of Syt appear to exert control over the likelihood of fusion pores undergoing rapid expansion, with the Syt-7 loops more often inhibiting pore expansion. Further insight can be drawn from the pH-switching experiment by Rao *et al.* (2014), in which kiss-and-run endocytosis was observed far more frequently for Syt-7 than Syt-1. Based on this, it would be reasonable to predict that the Syt1:7 chimeras (particularly Syt1:7-C2B$_{1,2,3}$) would also show higher rates of kiss-and-run endocytosis compared to WT Syt-1, although this remains to be tested.

Computer simulations and empirical work have suggested that changes in P+2S can also be used to assess whether fusion pores are expanding or remaining constricted. In theory, P+2S values should correspond to the relative dye concentration in a region confounded with the depth of that region within the evanescent field. Based on this, exocytotic events characterized by a persistently constricted fusion pore and/or endocytosis would be predicted to show an increase in P+2S, while events that undergo fusion pore expansion should show a transient decrease in P+2S (see methods). In the current study, P+2S values were observed to increase following nearly all fusion events (~95%), including in WT controls. Furthermore, the durations of these changes were in some cases substantially different from the duration of P/S perturbations (data not shown). While several factors could influence this (including the state of the fusion pore or depth of endocytosed vesicles), the most likely explanation might be based on the fact that DiD, in some cases, exhibited photoactivation during image acquisition. This could be seen in the corresponding raw image stacks, and occasionally resulted in intensity versus time plots where P+2S steadily increased from the beginning until the end of the imaging period. However,

photoactivation of DiD should not have influenced P/S ratios, as both *p*- and *s*-pol elicited emissions would change proportionately when this occurred.

The relationship between pHl persistence and P/S curvature could lead one to question whether this correlation was simply a byproduct of bleed through fluorescence signatures between imaging channels (488 nm, 561 nm *p*, 561 nm *s*). However, this was not the case, as emission spectra for pHl and DiD are highly divergent, with nearly no pHl emission exceeding 600 nm, and the lowest wavelength DiD emission beginning at ~625 nm (Shen *et al.*, 2014; Invitrogen Corporation, Carlsbad, CA). Additionally, the signals for pHl and DiD often differed considerably in duration for individual events and could be readily distinguished in raw images (e.g. pHl would be elevated for 3.6 sec, while P/S remained high for 45.6 sec). This uncoupling was observed with all constructs, and suggests that while Syt persistence might contribute to maintaining membrane curvature, the two parameters are not always in tight temporal synchronization.

The C2B domain of Syt has been previously implicated in influencing fusion pore dynamics. Wang *et al.* (2006) found that a point mutation in the third Syt-1 C2B loop, D363N, resulted in ~50% fewer fusion events in which the fusion pore dilated after forming. The mutation utilized in the Wang *et al.* study effectively neutralizes one of the conserved aspartic acid (D) residues found in the Ca^{2+}-binding pocket of both WT Syt-1 and Syt-7. Data from the current study suggests that other non-conserved amino acid residues in the Ca^{2+}-binding pocket can also impact the ability of Syt C2B to influence fusion pore dilation. One potential source for this influence is the adjacent residue at position 364. Syt-1 possesses a tyrosine (Y) residue in this position containing a hydrophobic, aromatic side chain, while Syt-7 (and therefore chimeras Syt1:7-C2B$_3$ and Syt1:7-C2B$_{1,2,3}$) has a lysine (K) residue with a hydrophilic, positively-charged side

chain (Figure 2.2). The differential properties of these amino acid side chains could theoretically result in proteins with the K364 genotype forming tighter electrostatic interactions with negatively-charged lipids (e.g. PIP_2, Phosphatidylcholine, Phosphatidylserine) near the fusion pore.

Further insight can be drawn from the presumptive location of the additional Ca^{2+} binding site in Syt-7 C2B (Figure 1.5). This third binding site is the result of contributions from a serine (S) and arginine (R) residue within C2B loop 3 (positions 368 and 369 respectively in Figure 2.2). These positions in Syt-1 are occupied by a glycine (G) and lysine (K) residue respectively. The substitution of these two amino acids (particularly the hydroxyl-containing serine) in Syt1:7-$C2B_3$ and Syt1:7-$C2B_{1,2,3}$, may underlie the significantly lower likelihood of their fusion pores to rapidly collapse (Figure 3.3; Table 3.3).

Xue *et al.* (2010) performed a similar Syt chimera study in Syt-1 knockout neurons with a slightly different approach than the present study. They first generated a chimera in which the Syt-1 C2B domain was replaced entirely with the Syt-7 C2B domain, and then introduced mutations that reverted portions of the domain back to their Syt-1 genotype. Replacing the entire C2B domain resulted in a significant reduction in the amplitude of post-synaptic electrical signaling (consistent with a decrease in rapid full-collapse fusion events typical of WT Syt-1). None of the reversions they introduced into C2B could rescue the loss of the robust rapid fusion component. However, it is interesting to note that this study specifically avoided reverting the C2B Ca^{2+}-binding loops, lending further support to the idea that these loops play a role in governing fusion mode.

Studies have also established the ability of Syt C2B to undergo partial membrane penetration via insertion of critical hydrophobic residues into the plasma membrane (Bai *et al.*, 2002; Fernandez-Chacon *et al.*, 2002; Bai *et al.*, 2004a). In Syt-1, these residues are valine (V) and isoleucine (I) at positions 304 (loop 1) and 367 (loop 3), respectively. Interestingly, Syt-7 has substitutions at both positions (V304I and I367L), and although the substituted amino acids are also hydrophobic, they may still differ in their degree of penetration and relative affinity based on their structural differences. Bai *et al.* (2002) showed *in vitro* that Syt-1 C2B membrane penetration is only enabled by the presence of the C2A domain, and other more recent studies have suggested that it is isoform-specific differences in C2A, rather than C2B, that underlie the disparate membrane binding characteristics of Syt-1 and Syt-7 (Brandt *et al.*, 2012; Vermaas & Tajkhorshid, 2017). Therefore, additional experiments using C2A chimeras should be conducted to address the relative contributions of these domains to membrane handling.

Homo-oligomerization is another commonly reported property of Syt that might explain the observed differences in persistence and fusion pore stability. As the role of Syt in triggering exocytosis began to be studied, one of the first observations researchers made was that Syt could form homo-oligomers in the presence of Ca^{2+} and anionic phospholipids, and that this property was specifically dependent on the C2B domain (Sugita *et al.*, 1996; Chapman *et al.*, 1996; Wu *et al.*, 2003; but also see Ubach *et al.*, 2001). Therefore, differences in the C2B sequence between Syt-1 and -7 might translate into differences in how avidly these isoforms aggregate with themselves. For example, multiple studies have shown that point mutations altering select tyrosine (Y) or lysine (K) residues in the Syt-1 C2B domain impede oligomerization and overall exocytosis *in vitro* (Chapman *et al.*, 1998; Littleton *et al.*, 2001). As noted above, a potentially

significant substitution in the Syt1:7-C2B$_3$ chimera is the Y364K mutation, which might have a similar influence on oligomerization of Syt surrounding fusion pores. Evidence also shows that Syt can form oligomers in a Ca^{2+}-independent manner, potentially through N-terminal interactions (Bai *et al.*, 2000; Wang *et al.*, 2014). Although in theory this interaction could affect fusion dynamics, the data presented in the current study only support a role for C2B-mediated interactions, as the N-termini of all chimeras were left unchanged from their Syt-1 parent DNA.

Oligomerization of Syt has also been implicated as a means for clustering other vital components of the fusion machinery. In the presence of Ca^{2+}, Syt-1 can bind the t-SNARE proteins Syntaxin and SNAP-25, and these interactions have been shown to be C2B-dependent and critical for exocytosis to proceed correctly (Sollner *et al.*, 1993; Chapman *et al.*, 1995; Chapman *et al.*, 1996; Zhang *et al.*, 2002; Bai *et al.*, 2004b; Lynch *et al.*, 2008). Therefore, it has been suggested that Syt C2B-mediated oligomerization might create a scaffold for the recruitment and proper assembly of SNARE complexes between the vesicle and plasma membrane *in vivo* (Littleton *et al.*, 2001). Furthermore, Syt-SNARE binding also appears to influence fusion pore stability, as impairment of t-SNARE binding inhibits fusion pore expansion and promotes kiss-and-run exocytosis (Lynch *et al.*, 2008). This raises the question of whether Syt-1 and Syt-7 differ in their affinity for binding SNAREs. For example, the tendency of chimeras Syt1:7-C2B$_3$ and Syt1:7-C2B$_{1,2,3}$ (as well as WT Syt-7) to mediate events in which the fusion pore fails to rapidly expand could be partially due to weaker interactions with SNARE complexes.

Even in the absence of oligomerization, interactions between molecules of Syt and other effector proteins can alter fusion pore stability. Research shows that Syt-1 can directly bind Complexin (Cpx) -1 and -2 associated with SNARE complexes, and that this interaction is

enhanced by Ca^{2+} (Tokumaru *et al.*, 2008; Xu *et al.*, 2013; Dhara *et al.*, 2014). Current models suggest that Cpx acts as a fusion clamp, binding the SNARE complex to prevent premature exocytosis, and that Syt might displace or induce conformational changes in Cpx to release the clamp and promote fusion. Cpx overexpression has also been shown to impede fusion pore expansion – an effect that is mimicked by Syt-1 knockout in chromaffin cells (Dhara *et al.*, 2014). These findings paint a picture in which Cpx and Syt-1 work in opposition to one another to either stabilize or destabilize the fusion pore, respectively. However, interactions between Cpx and Syt-7 have not been well characterized, raising the possibility that Syt-7 is more permissive of Cpx-mediated fusion pore restriction than Syt-1.

How and why would organisms use multiple Synaptotagmin isoforms that impart divergent outcomes on secretory vesicles? Perhaps the best possibility is that Syt-1 and Syt-7 are used to fine tune the energetic costs of secretion from adrenal chromaffin cells based on the current environmental context. Mild sympathetic nervous system (SNS) activity should favor secretion from Syt-7 vesicles, whereas robust SNS activation during periods of stress should also promote Syt-1 secretion (Fulop & Smith, 2007; Rao *et al.*, 2014). The advantage of this scheme is that mild Syt-7 release (presumably constituting the majority of an organism's life) would be characterized more often by a constricted fusion pore and kiss-and-run exocytosis, where only a limited amount of cargo (primarily small catecholamines versus larger neuropeptides) would be released into the circulatory system. Additionally, the structural components of the vesicle (i.e. phospholipids and integral proteins) would remain largely intact and capable of rapid recycling for additional rounds of exocytosis (Fulop *et al.*, 2005). However, when a stressful circumstance is perceived, the adrenal glands would be able to quickly effect physiological changes by

emptying the full contents of vesicles into the blood stream via a rapidly expanding fusion pore. Furthermore, the current study provides evidence that relatively small genetic alterations in critical domains of Syt can lead to gradated changes in the secretory phenotype. This may therefore highlight a path for past and future evolutionary diversification of Syt isoforms in other tissues.

Aside from chromaffin cells, Syt diversity could play a regulatory role in other cell types. For example, hippocampal neurons are known to express both Syt-1 and Syt-7, and it has been shown that stress induces changes in mRNA levels of Syt in hippocampal tissue (Sugita *et al.*, 2001; Thome *et al.*, 2001). Deficits in learning and memory function are well-characterized effects of chronic stress, and are likely due to impairment of long-term potentiation (LTP) in the hippocampus (Kim *et al.*, 1996). One mechanism implicated in the process of LTP is modulation of presynaptic fusion pores. Specifically, this theory suggests that the conversion of glutamate-associated fusion events from a non-expanding to rapidly expanding pore phenotype increases the signaling activity at a given synapse (the definition of LTP) by activating an additional postsynaptic receptor type (Choi *et al.*, 2000; Choi *et al.*, 2003). Therefore, an attractive hypothesis would be that LTP in the hippocampus results from a combination of down-regulating Syt-7 and/or up-regulating Syt-1 to modify the predominant fusion pore phenotype.

Conclusions

The current study provides evidence that the Synaptotagmin C2B domain Ca^{2+}-binding loops influence the persistence of Syt at fusion sites and the likelihood of vesicle fusion pores undergoing rapid expansion during exocytosis. This was investigated in living chromaffin cells through polarized TIRF microscopy using chimeric Syt proteins in which the C2B loops of Syt-1

were replaced by those of Syt-7. Substitution of all three C2B loops resulted in a pronounced shift in the Syt-1 phenotype towards that of WT Syt-7. However, this did not fully account for the difference observed between wild-type isoforms, suggesting that other domains should be investigated for their relative contribution to these behaviors. Additionally, future research should address whether swapping the C2B loops also leads to higher rates of kiss-and-run exocytosis and slowing of cargo release, as has been documented for WT Syt-7. Nonetheless, the results presented here provide novel and important insights into how Synaptotagmin, a protein previously thought to act only in the steps leading up to fusion, may also play a role in the molecular regulation of fusion pore expansion during the later stages of exocytosis.

REFERENCES

Ahras, M., Otto, G., and Tooze, S. (2006). Synaptotagmin IV is necessary for the maturation of secretory granules in PC12 cells. *Journal of Cell Biology, 173*(2), 241-251.

Alberts, B., Johnson, A., Lewis, J., Raff, M., Roberts, K., and Walter, P. (2008). *Molecular Biology of the Cell.* New York, NY: Garland Science.

Anantharam, A., Onoa, B., Edwards, R., Holz, R., and Axelrod, D. (2010). Localized topological changes of the plasma membrane upon exocytosis visualized by polarized TIRFM. *The Journal of Cell Biology, 188*(3), 415-428.

Anantharam, A., Axelrod, D., and Holz, R. (2012). Real-time imaging of plasma membrane deformations reveals pre-fusion membrane curvature changes and a role for dynamin in the regulation of fusion pore expansion. *Journal of Neurochemistry, 122*, 661-671.

Axelrod, D. (1979). Carbocyanine dye orientation in red cell membrane studied by microscopic fluorescence polarization. *Biophysical Journal, 26*, 557-574.

Axelrod, D., Burghardt, T., and Thompson, N. (1984). Total internal reflection fluorescence. *Annual Review of Biophysics and Bioengineering, 13*, 247-268.

Bacaj, T., Wu, D., Yang, X., Morishita, W., Zhou, P., Xu, W., Malenka, R., and Sudhof, T. (2013). Synaptotagmin-1 and synaptotagmin-7 trigger synchronous and asynchronous phases of neurotransmitter release. *Neuron, 80*, 947-959.

Bader, M., Holz, R., Kumakura, K., and Vitale, N. (2002). Exocytosis: the chromaffin cell as a model system. *Annals of the New York Academy of Sciences, 971*, 178-183.

Bai, J., Earles, C., Lewis, J., and Chapman, E. (2000). Membrane-embedded synaptotagmin penetrates cis or trans target membranes and clusters via a novel mechanism. *The Journal of Biological Chemistry, 275*(33), 25427-25435.

Bai, J., Wang, P., and Chapman, E. (2002). C2A activates a cryptic Ca^{2+}-triggered membrane penetration activity within the C2B domain of synaptotagmin I. *Proceedings of the National Academy of Sciences, 99*(3), 1665-1670.

Bai, J., and Chapman, E. (2004a). The C2 domains of synaptotagmin – partners in exocytosis. *Trends in Biochemical Sciences, 29*(3), 143-151.

Bai, J., Wang, C., Richards, D., Jackson, M., and Chapman, E. (2004b). Fusion pore dynamics are regulated by synaptotagmin-t-SNARE interactions. *Neuron, 41*, 929-942.

Banerjee, A., Barry, V., DasGupta, B., and Martin, T. (1996). N-ethylmaleimide-sensitive factor acts at a prefusion ATP-dependent step in Ca^{2+}-activated exocytosis. *The Journal of Biological Chemistry, 271*(34), 20223-20226.

Burgoyne, R., and Morgan, A. (1993). Regulated exocytosis. *Biochemical Journal, 293*, 305-316.

Bhalla, A., Tucker, W., and Chapman, E. (2005). Synaptotagmin isoforms couple distinct ranges of Ca^{2+}, Ba^{2+}, and Sr^{2+} concentration to SNARE-mediated membrane fusion. *Molecular Biology of the Cell, 16*, 4755-4764.

Bhalla, A., Chicka, M., Tucker, W., and Chapman, E. (2006). Ca^{2+}-synaptotagmin directly regulates t-SNARE function during reconstituted membrane fusion. *Nature Structural & Molecular Biology, 13*(4), 323-330.

Brandt, D., Coffman, M., Falke, J., and Knight, J. (2012). Hydrophobic contributions to the membrane docking of synaptotagmin 7 C2A domain: mechanistic contrast between isoforms 1 and 7. *Biochemistry, 51*(39), 7654-7664.

Brose, N., Petrenko, A., Sudhof, T., and Jahn, R. (1992). Synaptotagmin: a calcium sensor on the synaptic vesicle surface. *Science, 256*, 1021-1025.

Carmichael, S., and Winkler, H. (1985). The adrenal chromaffin cell. *Scientific American, 253*(2), 40-49.

Chapman, E., Hanson, P., An, S., and Jahn, R. (1995). Ca^{2+} regulates the interaction between synaptotagmin and syntaxin 1. *The Journal of Biological Chemistry, 270*(40), 23667-23671.

Chapman, E., Blasi, J., An, S., Brose, N., Johnston, P., Sudhof, T., and Jahn, R. (1996a). Fatty acylation of synaptotagmin in PC12 cells and synaptosomes. *Biochemical and Biophysical Research Communications, 225*, 326-332.

Chapman, E., An, S., Edwardson, M., and Jahn, R. (1996b). A novel function for the second C2 domain of synaptotagmin. *The Journal of Biological Chemistry, 271*(10), 5844-5849.

Chapman, E., Desai, R., Davis, A., and Tornehl, C. (1998). Delineation of the oligomerization, AP-2 binding, and synprint binding region of the C2B domain of synaptotagmin. *The Journal of Biological Chemistry, 273*(49), 32966-32972.

Chapman, E. (2002). Synaptotagmin: a Ca^{2+} sensor that triggers exocytosis? *Nature Reviews, 3*, 1-11.

Chapman, E. (2008). How does synaptotagmin trigger neurotransmitter release? *Annual Reviews of Biochemistry, 77*, 615-641.

Chieregatti, E., Witkin, J., and Baldini, G. (2002). SNAP-25 and synaptotagmin 1 function in Ca^{2+}-dependent reversible docking of granules to the plasma membrane. *Traffic, 3*, 496-511.

Choi, S., Klingauf, J., and Tsien, R. (2000). Postfusional regulation of cleft glutamate concentration during LTP at 'silent synapses'. *Nature Neuroscience, 3*(4), 330-336.

Choi, S., Klingauf, J., and Tsien, R. (2003). Fusion pore modulation as a presynaptic mechanism contributing to expression of long-term potentiation. *Philosophical Transactions of the Royal Society of London B, 358*, 695-705.

Chow, R., von Ruden, L., and Neher, E. (1992). Delay in vesicle fusion revealed by electrochemical monitoring of single secretory events in adrenal chromaffin cells. *Nature, 356*, 60-63.

Chow, R., Klingauf, J., Heinemann, C., Zucker, R., and Neher, E. (1996). Mechanisms determining the time course of secretion in neuroendocrine cells. *Neuron, 16*, 369-376.

Coupland, R. (1989). The natural history of the chromaffin cell – twenty-five years on the beginning. *Archives of Histology and Cytology, 52*, 331-341.

de Wit, H., Cornelisse, L., Toonen, R., and Verhage, M. (2006). Docking of secretory vesicles is syntaxin dependent. *PLOS ONE, 1*, e126.

Dhara, M., Yarzagaray, A., Schwarz, Y., Dutta, S., Grabner, C., Moghadam, P., Bost, A., Schirra, C., Rettig, J., Reim, K., Brose, N., Mohrmann, R., and Bruns, D. (2014). Complexin synchronizes primed vesicle exocytosis and regulates fusion pore dynamics. *The Journal of Cell Biology, 204*(7), 1123-1140.

Fenwick, E., Marty, A., and Neher, E. (1982). A patch-clamp study of bovine chromaffin cells and of their sensitivity to acetylcholine. *The Journal of Physiology, 331*, 577-597.

Fernandez-Chacon, R., Shin, O., Konigstorfer, A., Matos, M., Meyer, A., Garcia, J., Gerber, S., Rizo, J., Sudhof, T., and Rosenmund, C. (2002). Structure/function analysis of Ca^{2+} binding to the C2A domain of synaptotagmin 1. *The Journal of Neuroscience, 22*(19), 8438-8446.

Fresce, R., Grohovaz, F., Valtorta, F., and Meldolesi, J. (1994). Neurotransmitter release: fusion or 'kiss-and-run'? *Trends in Cell Biology, 4*, 1-4.

Fukuda, M., Kowalchyk, J., Zhang, X., Martin, T., and Mikoshiba, K. (2001). Synaptotagmin IX regulates Ca^{2+}-dependent secretion in PC12 cells. *The Journal of Biological Chemistry, 277*(7), 4601-4604.

Fulop, T., Radabaugh, S., and Smith, C. (2005). Activity-dependent differential transmitter release in mouse adrenal chromaffin cells. *The Journal of Neuroscience, 25*(32), 7324-7332.

Fulop, T., and Smith, C. (2007). Matching native electrical stimulation by graded chemical stimulation in isolated mouse adrenal chromaffin cells. *Journal of Neuroscience Methods, 166*, 195-202.

Geppert, M., Goda, Y., Hammer, R., Li, C., Rosahl, T., Stevens, C., and Sudhof, T. (1994). Synaptotagmin I: a major Ca^{2+} sensor for transmitter release at a central synapse. *Cell, 79*, 717-727.

Greene, L., and Tischler, A. (1976). Establishment of a noradrenergic clonal line of rat adrenal pheochromocytoma cells which respond to nerve growth factor. *Proceedings of the National Academy of Sciences, 73*(7), 2424-2428.

Gulyas-Kovacs, A., de Wit, H., Milosevic, I., Kochubey, O., Toonen, R., Klingauf, J., Verhage, M., and Sorensen, J. (2007). *The Journal of Neuroscience, 27*(32), 8676-8686.

Gustavsson, N., and Han, W. (2009). Calcium-sensing beyond neurotransmitters: functions of synaptotagmins in neuroendocrine and endocrine secretion. *Bioscience Reports, 29*, 245-259.

Hagler, D., and Goda, Y. (2001). Properties of synchronous and asynchronous release during pulse train depression in cultured hippocampal neurons. *Journal of Neurophysiology, 85*(6), 2324-2334.

Harata, N., Aravanis, A., and Tsien, R. (2006). Kiss-and-run and full-collapse fusion as modes of exo-endocytosis in neurosecretion. *Journal of Neurochemistry, 97*, 1546-1570.

Hata, Y., Slaughter, C., and Sudhof, T. (1993). Synaptic vesicle fusion complex contains unc-18 homologue bound to syntaxin. *Nature, 366*, 347-351.

Hay, J., and Martin, T. (1993). Phosphatidylinositol transfer protein required for ATP-dependent priming of Ca^{2+}-activated secretion. *Nature, 366*, 572-575.

Hay, J., and Scheller, R. (1997). SNAREs and NSF in targeted membrane fusion. *Current Opinions in Cell Biology, 9*, 505-512.

Heuser, J., Reese, T., Dennis, M., Jan, Y., Jan, L., and Evans, L. (1979). Synaptic vesicle exocytosis captured by quick freezing and correlated with quantal transmitter release. *Journal of Cell Biology, 81*, 275-300.

Hirsch, D., and Zukowska, Z. (2012). NPY and stress 30 years later: the peripheral view. *Cellular and Molecular Neurobiology, 32*(5), 645-659.

Holz, R., Bittner, M., Peppers, S., Senter, R., and Eberhard, D. (1989). MgATP-independent and MgATP-dependent exocytosis. *The Journal of Biological Chemistry, 264*(10), 5412-5419.

Holz, R., Hlubek, M., Sorensen, S., Fisher, S., Balla, T., Ozaki, S., Prestwich, G., Stuenkel, E., and Bittner, M. (2000). A pleckstrin homology domain specific for PtdIns-4-5-P_2 and fused to green fluorescent protein identifies plasma membrane PtdIns-4-5-P_2 as being important in exocytosis. *The Journal of Biological Chemistry, 275*(23), 17878-17885.

Hui, E., Bai, J., Wang, P., Sugimori, M., Llinas, R., and Chapman, E. (2005). Three distinct kinetic groupings of the synaptotagmin family: candidate sensors for rapid and delayed exocytosis. *Proceedings of the National Academy of Sciences, 102*(14), 5210-5214.

Hui, E., Johnson, C., Yao, J., Dunning, F., and Chapman, E. (2009). Synaptotagmin-mediated bending of the target membrane is a critical step in Ca^{2+}-regulated fusion. *Cell, 138*, 709-721.

Kabachinski, G., Yamaga, M., Kielar-Grevstad, D., Bruinsma, S., and Martin, T. (2013). CAPS and munc13 utilize distinct PIP_2-linked mechanisms to promote vesicle exocytosis. *Molecular Biology of the Cell, 25*, 508-521.

Kaeser, P., and Regehr, W. (2014). Molecular mechanisms for synchronous, asynchronous, and spontaneous neurotransmitter release. *Annual Review of Physiology, 76*, 333-363.

Kavalali, E., and Jorgensen, E. (2014). Visualizing presynaptic function. *Nature Neuroscience, 17*, 10-16.

Kim, J., Foy, M., and Thompson, R. (1996). Behavioral stress modifies hippocampal plasticity through N-methyl-D-aspartate receptor activation. *Proceedings of the National Academy of Sciences, 93*, 4750-4753.

Klenchin, V., and Martin, T. (2000). Priming in exocytosis: attaining fusion-competence after vesicle docking. *Biochimie, 82*(5), 399-407.

Kolski-Andreaco, A., Cai, H., Currie, D., Chandy, K., and Chow, R. (2007). Mouse adrenal chromaffin cell isolation. *Journal of Visualized Experiments, 2*, e129.

Lefkowitz, J., DeCrescenzo, V., Duan, K., Bellve, K., Fogarty, K., Walsh, J., and ZhuGe, R. (2014). Catecholamine exocytosis during low frequency stimulation in mouse adrenal chromaffin cells is primarily asynchronous and controlled by the novel mechanism of Ca^{2+} syntilla suppression. *The Journal of Physiology, 592*(21), 4639-4655.

Li, C., Ullrich, B., Zhang, J., Anderson, R., Brose, N., and Sudhof, T. (1995). Ca^{2+}-dependent and -independent activities of neural and non-neural synaptotagmins. *Nature, 375*(6532), 594-599.

Littleton, J., Bai, J., Vyas, B., Desai, R., Baltus, A., Garment, M., Carlson, S., Ganetzky, B., and Chapman, E. (2001). Synaptotagmin mutants reveal essential functions for the C2B domain in Ca^{2+}-triggered fusion and recycling of synaptic vesicles in vivo. *The Journal of Neuroscience, 21*(5), 1421-1433.

Lundberg, J., Hamberger, B., Schultzberg, M., Hokfelt, T., Granberg, P., Efendic, S., Terenius, L., Goldstein, M., and Luft, R. (1979). Enkephalin- and somatostatin-like immunoreactivities in human adrenal medulla and pheochromocytoma. *Proceedings of the National Academy of Sciences, 76*(8), 4079-4083.

Lynch, K., Gerona, R., Kielar, D., Martens, S., McMahon, H., and Martin, T. (2008). Synaptotagmin-1 utilizes membrane bending and SNARE binding to drive fusion pore expansion. *Molecular Biology of the Cell, 19*, 5093-5103.

Mackler, J., Drummond, J., Loewen, C., Robinson, I., and Reist, N. (2002). The C2B Ca^{2+}-binding motif of synaptotagmin is required for synaptic transmission in vivo. *Nature, 418*, 340-344.

Martens, S., Kozlov, M., and McMahon, H. (2007). How synaptotagmin promotes membrane fusion. *Science, 316*(5828), 1205-1208.

Martin, T. (2012). Role of $PI(4,5)P_2$ in vesicle exocytosis and membrane fusion. *Subcellular Biochemistry, 59*, 111-130.

Miesenbock, G., De Angelis, D., and Rothman, J. (1998). Visualizing secretion and synaptic transmission with pH-sensitive green fluorescent proteins. *Nature, 394*, 192-195.

Ockenga, W. (2012). Total internal reflection fluorescence (TIRF) microscopy. *Science Lab by Leica Microsystems*. Accessed 5 June 2017. <http://www.leica-microsystems.com/science-lab/total-internal-reflection-fluorescence-tirf-microscopy/>

Palfreyman, M., and Jorgensen, E. (2008). Chapter 3: Roles of SNARE proteins in synaptic vesicle fusion. In Z.W. Wang (Ed.), *Molecular Mechanisms of Neurotransmitter Release* (pp. 35-59). New York, NY: Humana Press.

Perin, M., Fried, V., Mignery, G., Jahn, R., and Sudhof, T. (1990). Phospholipid binding by a synaptic vesicle protein homologous to the regulatory region of protein kinase C. *Nature, 345*(6272), 260-263.

Rao, T., Passmore, D., Peleman, A., Das, M., Chapman, E., and Anantharam, A. (2014). Distinct fusion properties of synaptotagmin-1 and synaptotagmin-7 bearing dense core granules. *Molecular Biology of the Cell, 25*, 2416-2427.

Rao, T. (2016). Role of secretory granule heterogeneity in calcium-triggered exocytosis. *Wayne State University Dissertations,* Paper 1579.

Rao, T., Rodriguez, Z., Bradberry, M., Ranski, A., Dahl, P., Schmidtke, M., Jenkins, P., Axelrod, D., Chapman, E., Giovannucci, D., and Anantharam, A. (2017). Synaptotagmin isoforms confer distinct activation kinetics and dynamics to chromaffin cell granules. *The Journal of General Physiology, 149*(8).

Rothman, J. (1994). Mechanisms of intracellular protein transport. *Nature, 372*(6501), 55-63.

Schonn, J., Maximov, A., Lao, Y., Sudhof, T., and Sorensen, J. (2008). Synaptotagmin-1 and -7 are functionally overlapping Ca^{2+} sensors for exocytosis in adrenal chromaffin cells. *Proceedings of the National Academy of Sciences, 105*(10), 3998-4003.

Segovia, M., Ales, E., Montes, M., Bonifas, I., Jemal, I., Lindau, M., Maximov, A., Sudhof, T., and Alvarez de Toledo, G. (2010). Push-and-pull regulation of the fusion pore by synaptotagmin-7. *Proceedings of the National Academy of Sciences, 107*(44), 19032-19037.

Shao, X., Davletov, B., Sutton, R., Sudhof, T., and Rizo, J. (1996). Bipartite Ca^{2+}-binding motif in C2 domains of synaptotagmin and protein kinase C. *Science, 273*, 248-251.

Shen, Y., Rosendale, M., Campbell, R., and Perrais, D. (2014). pHuji, a pH-sensitive red fluorescent protein for imaging of exo- and endocytosis. *The Journal of Cell Biology, 207*(3), 419-432.

Smith, C., and Eiden, L. (2012). Is PACAP the major neurotransmitter for stress transduction at the adrenomedullary synapse? *Journal of Molecular Neuroscience, 48*(2), 403-412.

Sollner, T., Bennett, M., Whiteheart, S., Scheller, R., and Rothman, J. (1993). A protein assembly-disassembly pathway in vitro that may correspond to sequential steps of synaptic vesicle docking, activation, and fusion. *Cell, 75*, 409-418.

Steyer, J., Horstmann, H., and Almers, W. (1997). Transport, docking and exocytosis of single secretory granules in live chromaffin cells. *Nature, 388*, 474-478.

Striegel, A., Biela, L., Evans, C., Wang, Z., Delehoy, J., Sutton, R., Chapman, E., and Reist, N. (2012). Calcium binding by synaptotagmin's C2A domain is an essential element of the electrostatic switch that triggers synchronous synaptic transmission. *The Journal of Neuroscience, 32*(4), 1253-1260.

Sudhof, T., and Rizo, J. (1996). Synaptotagmins: C2-domain proteins that regulate membrane traffic. *Neuron, 17*, 379-388.

Sudhof, T. (2002). Synaptotagmins: why so many? *The Journal of Biological Chemistry, 277*(10), 7629-7632.

Sudhof, T., and Rothman, J. (2009). Membrane fusion: grappling with SNARE and SM proteins. *Science, 323*(5913), 474-477.

Sugita, S., Hata, Y., and Sudhof, T. (1996). Distinct Ca^{2+}-dependent properties of the first and second C2-domains of synaptotagmin I. *The Journal of Biological Chemistry, 271*(3), 1262-1265.

Sugita, S., Han, W., Butz, S., Liu, X., Fernandez-Chacon, R., Lao, Y., and Sudhof, T. (2001). Synaptotagmin VII as a plasma membrane Ca^{2+} sensor in exocytosis. *Neuron, 30*, 459-473.

Sugita, S., Shin, O., Han, W., Lao, Y., and Sudhof, T. (2002). Synaptotagmins form a hierarchy of exocytotic Ca^{2+} sensors with distinct Ca^{2+} affinities. *The European Molecular Biology Organization Journal, 21*(3), 270-280.

Sutton, R., Davletov, B., Berghuis, A., Sudhof, T., and Sprang, S. (1995). Structure of the first C2 domain of synaptotagmin I: a novel Ca^{2+}/phospholipid-binding fold. *Cell, 80*, 929-938.

Sutton, R., Fasshauer, D., Jahn, R., and Brunger, A. (1998). Crystal structure of a SNARE complex involved in synaptic exocytosis at 2.4Å resolution. *Nature, 395*, 347-353.

Taraska, J., Perrais, D., Ohara-Imaizumi, M., Nagamatsu, S., and Almers, W. (2003). Secretory granules are recaptured largely intact after stimulated exocytosis in cultured endocrine cells. *Proceeding of the National Academy of Sciences, 100*(4), 2070-2075.

Taraska, J., and Almers, W. (2004). Bilayers merge even when exocytosis is transient. *Proceedings of the National Academy of Sciences, 101*(23), 8780-8785.

Thome, J., Pesold, B., Baader, M., Hu, M., Gewirtz, J., Duman, R., and Henn, F. (2001). Stress differentially regulates synaptophysin and synaptotagmin expression in hippocampus. *Biological Psychiatry, 50*(10), 809-812.

Tokumaru, H., Shimizu-Okabe, C., and Abe, T. (2008). Direct interaction of SNARE complex binding protein synaphin/complexin with calcium sensor synaptotagmin I. *Brain Cell Biology, 36*, 173-189.

Tucker, W., Edwardson, J., Bai, J., Kim, H., Martin, T., and Chapman, E. (2003). Identification of synaptotagmin effectors via acute inhibition of secretion from cracked PC12 cells. *The Journal of Cell Biology, 162*(2), 199-209.

Tucker, W., and Chapman, E. (2002). Role of synaptotagmin in Ca^{2+}-triggered exocytosis. *Biochemical Journal, 366*, 1-13.

Ubach, J., Lao, Y., Fernandez, I., Arac, D., Sudhof, T., and Rizo, J. (2001). The C2B domain of synaptotagmin I is a Ca^{2+}-binding module. *Biochemistry, 40*, 5854-5860.

Verhage, M., and Sorensen, J. (2008). Vesicle docking in regulated exocytosis. *Traffic, 9*, 1414-1424.

Vermaas, J., and Tajkhorshid, E. (2017). Differential membrane binding mechanics of synaptotagmin isoforms observed in atomic detail. *Biochemistry, 56*, 281-293.

Voets, T., Neher, E., and Moser, T. (1999). Mechanisms underlying phasic and sustained secretion in chromaffin cells from mouse adrenal slices. *Neuron, 23*, 607-615.

Voets, T., Moser, T., Lund, P., Chow, R., Geppert, M., Sudhof, T., and Neher, E. (2001a). Intracellular calcium dependence of large dense-core vesicle exocytosis in the absence of synaptotagmin I. *Proceedings of the National Academy of Sciences, 98*(20), 11680-11685.

Voets, T., Toonen, R., Brian, E., de Wit, H., Moser, T., Rettig, J., Sudhof, T., Neher, E., and Verhage, M. (2001b). Munc18-1 promotes large dense-core vesicle docking. *Neuron, 31*, 581-591.

Wang, C., Grishanin, R., Earles, C., Chang, P., Martin, T., Chapman, E., and Jackson, M. (2001). Synaptotagmin modulation of fusion pore kinetics in regulated exocytosis of dense-core vesicles. *Science, 294*, 1111-1115.

Wang, C., Bai, J., Chang, P., Chapman, E., and Jackson, M. (2006). Synaptotagmin-Ca^{2+} triggers two sequential steps in regulated exocytosis in rat PC12 cells: fusion pore opening and fusion pore dilation. *The Journal of Physiology, 570*(2), 295-307.

Wang, J., Bello, O., Auclair, S., Wang, J., Coleman, J., Pincet, F., Krishnakumar, S., Sindelar, C., and Rothman, J. (2014). Calcium sensitive ring-like oligomers formed by synaptotagmin. *Proceedings of the National Academy of Sciences, 111*(38), 13966-13971.

Wiedemann, C., Schafer, T., and Burger, M. (1996). Chromaffin granule-associated phosphatidylinositol 4-kinase activity is required for stimulated secretion. *The European Molecular Biology Organization Journal, 15*(9), 2094-2101.

Wu, Y., He, Y., Bai, J., Ji, S., Tucker, W., Chapman, E., and Sui, S. (2003). Visualization of synaptotagmin I oligomers assembled onto lipid monolayers. *Proceedings of the National Academy of Sciences, 100*(4), 2082-2087.

Xu, T., Ashery, U., Burgoyne, R., and Neher, E. (1999). Early requirement for α-SNAP and NSF in the secretory cascade in chromaffin cells. *The European Molecular Biology Organization Journal, 18*(12), 3293-3304.

Xu, J., Brewer, K., Perez-Castillejos, R., and Rizo, J. (2013). Subtle interplay between synaptotagmin- and complexin-binding to the SNARE complex. *Journal of Molecular Biology, 425*(18), 3461-3475.

Xue, M., Craig, T., Shin, O., Li, L., Brautigam, C., Tomchick, D., Sudhof, T., Rosenmund, C., and Rizo, J. (2010). Structural and mutational analysis of functional differentiation between synaptotagmins-1 and -7. *PLOS ONE, 5*(9), e12544.

Yoshihara, M., Guan, Z., and Littleton, T. (2010). Differential regulation of synchronous versus asynchronous neurotransmitter release by the C2 domains of synaptotagmin 1. *Proceedings of the National Academy of Sciences, 107*(33), 14869-14874.

Zhang, X., Rizo, J., and Sudhof, T. (1998). Mechanism of phospholipid binding by the C2A-domain of synaptotagmin I. *Biochemistry, 37*, 12395-12403.

Zhang, X., Kim-Miller, M., Fukuda, M., Kowalchyk, J., and Martin, T. (2002). Ca^{2+}-dependent synaptotagmin binding to SNAP-25 is essential for Ca^{2+}-triggered exocytosis. *Neuron, 34*, 599-611.

Zhang, Z., Wu, Y., Wang, Z., Dunning, F., Rehfuss, J., Ramanan, D., Chapman, E., and Jackson, M. (2011). Release mode of large and small dense-core vesicles specified by different synaptotagmin isoforms in PC12 cells. *Molecular Biology of the Cell, 22*, 2324-2336.

Zucker, R., Kullmann, D., and Kaeser, P. (2014). Release of Neurotransmitters. In Byrne, J., Heidelberger, R., and Waxham, M. (Eds.), *From Molecules to Networks* (pp. 443-488). Amsterdam, Netherlands: Elsevier Inc.

ABSTRACT

SYNAPTOTAGMIN C2B CA^{2+}-BINDING LOOPS IMPOSE DISTINCT EXOCYTOSIS PHENOTYPES

by

MICHAEL W. SCHMIDTKE

August 2017

Advisor: Dr. Karen Beningo

Major: Biological Sciences (Cellular, Developmental, & Neurobiology)

Degree: Master of Science

Regulated exocytosis from chromaffin cells in the adrenal medulla plays a critical role in maintaining organismal homeostasis. In the absence of stress, these cells release physiologically relevant substances into the blood stream only in limited quantities, whereas stressful conditions result in a rapid deluge of signaling molecules used, for example, to increase heart rate and pain tolerance. Although the cellular mechanisms governing the switch from low-level to stress-induced secretion are not well understood, recent evidence has implicated the exocytotic Ca^{2+}-sensing protein Synaptotagmin (Syt) in this role.

Two isoforms of Syt are expressed in chromaffin cells (Syt-1 and Syt-7), and each is sorted to a different secretory vesicle population. Fusion events mediated by Syt-7 occur under milder stimulation conditions and result in slower release of vesicle cargo through a narrow fusion pore that often reseals ("kiss-and-run" exocytosis). Conversely, Syt-1 events require stronger cellular stimulation (characteristic of a stress response) and typically result in vesicles fully collapsing into the plasma membrane to rapidly release all cargo. Furthermore, Syt-7 remains clustered at fusion sites while Syt-1 rapidly diffuses away.

Although the distinct phenotypes of Syt-1 and Syt-7 may explain how chromaffin cells tune their secretory response to deal with intermittent periods of stress, a significant gap in this field is understanding the intermolecular basis for these phenotypic differences. The current study aimed to address this gap by using polarized Total Internal Reflection Fluorescence (pTIRF) microscopy to compare the phenotypes of various Syt chimeras, containing portions of both Syt-1 and Syt-7, with the behavior of the wild-type (WT) proteins. The Ca^{2+}-binding loops of the Syt C2B domain were a prime candidate to target based on this domain's established role in exocytosis and Ca^{2+}-mediated interactions with other molecules. Chimeras composed of a Syt-1 background with individual C2B loops converted to match Syt-7 showed a mild increase in Syt persistence at fusion sites and slight inhibition of fusion pore expansion when compared to WT Syt-1. These effects were enhanced substantially when all three C2B loops were converted to the Syt-7 genotype, suggesting that the coordinated action of these loops serves as a major determinant of the exocytotic fusion mode.

AUTOBIOGRAPHICAL STATEMENT

MICHAEL W. SCHMIDTKE

Michael received his Bachelor of Science in 2011 from the University of Michigan – Ann Arbor with a concentration in ecology and evolutionary biology. Following graduation, he worked as an ecological field research technician and volunteered in the mammals division at the University of Michigan Museum of Natural History. He also spent time working as a biological science technician for the U.S. Forest Service in 2013. Michael's interest in behavioral endocrinology and stress led him to Wayne State University in the fall of 2014 to study the molecular mechanics of adrenal gland secretion.